J|A|C|S
ARTICLES
Published on Web 07/22/2006

Construction of Segregated Arrays of Multiple Donor and Acceptor Units Using a Dendritic Scaffold: Remarkable Dendrimer Effects on Photoinduced Charge Separation

Wei-Shi Li,*,† Kil Suk Kim,§ Dong-Lin Jiang,† Hiroyuki Tanaka,# Tomoji Kawai,# Jung Ho Kwon,§ Dongho Kim,*,§ and Takuzo Aida*,†,‡

Contribution from the ERATO-SORST Nanospace Project, Japan Science and Technology Agency (JST), National Museum of Emerging Science and Innovation, 2-41 Aomi, Koto-ku, Tokyo 135-0064, Japan, The Institute of Scientific and Industrial Research (ISIR), Osaka University, 8-1, Mihogaoka, Ibaragi, Osaka 567-0047, Japan, National Creative Research Initiatives, Center for Ultrafast Optical Characteristics Control and Department of Chemistry, Yonsei University, Seoul 120-749, Korea, and Department of Chemistry and Biotechnology, School of Engineering, and Center for NanoBio Integration, The University of Tokyo, 7-3-1 Hongo, Bunkyo-ku, Tokyo 113-8656, Japan

Received May 3, 2006; E-mail: li@nanospace.miraikan.jst.go.jp; dongho@yonsei.ac.kr; aida@macro.t.u-tokyo.ac.jp

Abstract: Dendritic molecules appended with multiple zinc porphyrin units (DP_m, *m* [number of zinc porphyrin units] = 6, 12, and 24) trap bipyridine compounds carrying multiple fullerene units (Py_2F_n, *n* [number of C_{60} units] = 1−3), affording coordination complexes $DP_m \supset Py_2F_n$ having a photoactive layer consisting of spatially segregated donor and acceptor arrays on their surface. Complexes $DP_m \supset Py_2F_n$ are stable enough (*K* [average binding affinity] = 1.1×10^6−4.4×10^6 M^{-1} in $CHCl_3$ at 25 °C) to be isolated by gel permeation chromatography. UHV−STM microscopy enables clear visualization of a petal-like structure of $DP_{12} \supset Py_2F_3$. Photoexcitation of the zinc porphyrin units in $DP_m \supset Py_2F_n$ results in a zinc porphyrin-to-fullerene electron transfer to generate a charge separation. The charge-separation rate constant (k_{CS}) in CH_2Cl_2 at 20 °C increases from 0.26×10^{10} to 2.3×10^{10} s^{-1} upon increment of *m* and *n*, whereas the charge-recombination rate constant (k_{CR}) remains almost unchanged at 4.5×10^6−6.7×10^6 s^{-1}. Consequently, $DP_{24} \supset Py_2F_3$ furnishes the largest ratio of k_{CS}/k_{CR} (3400) among the family.

Introduction

In biological photosynthesis, photoinduced electron transfer (PET) is one of the most essential events for conversion of solar energy into chemical energy. Molecular design of artificial photosynthetic systems involving restricted spatial arrangements of covalently[1] and noncovalently[2] linked electron donor (D) and acceptor (A) units has long been a central interest and now attracts even greater attention for the development of optoelectronic devices such as solar cells.[3] For the fabrication of those materials, charge-transfer complexations between D and A units, leading to rapid quenching of charge-carrier transports, must be avoided, while D and A units are required to assemble individually to form their segregated arrays.[4] Having this context in mind, we were motivated to achieve at the molecular level such segregated arrays of multiple D and A units. Although a variety of D/A systems having multiple D or A units have been reported,[5] those containing large numbers of both D and A units are unprecedented. In the present paper, we report novel photofunctional dendrimers consisting of spatially segregated arrays of multiple D and A units on their surface.

Our molecular design strategy (Scheme 1) made use of petal-like dendritic structures as scaffolds[6] to realize a wheel-like or spherical arrangement of multiple zinc porphyrin (P) units (DP_m; m = 6, 12, and 24),[7] which are capable of ligating multiple molecules of bipyridine compounds having 1−3 fullerene (F) units (Py_2F_n; n = 1−3). Since the zinc porphyrin moieties in DP_m are located in the outermost dendritic layer, and the

† ERATO-SORST Nanospace Project, JST.
‡ The University of Tokyo.
§ Yonsei University; responsible for time-resolved spectroscopies.
# Osaka University; responsible for scanning tunneling microscopy.

(1) For books and reviews: (a) Kavarnos, G. J. *Fundamentals of Photoinduced Electron Transfer*; VCH: New York, 1993. (b) Wasielewski, M. R. *Chem. Rev.* **1992**, *92*, 435−461. (c) Gust, D.; Moore, T. A.; Moore, A. L. *Acc. Chem. Res.* **2001**, *34*, 40−48. (d) Guldi, D. M. *Chem. Soc. Rev.* **2002**, *31*, 22−36. (e) Imahori, H. *Org. Biomol. Chem.* **2004**, *2*, 1425−1433.
(2) For reviews: (a) El-Khously, M. E.; Ito, O.; Smith, P. M.; D'Souza, F. *J. Photochem. Photobiol., C* **2004**, *5*, 79−104. (b) D'Souza, F.; Ito, O. *Coord. Chem. Rev.* **2005**, *249*, 1410−1422.
(3) (a) Nunzi, J.-M. *C. R. Phys.* **2002**, *3*, 523−542. (b) Gregg, B. A. *J. Phys. Chem. B* **2003**, *107*, 4688−4698. (c) Grätzel, M. *J. Photochem. Photobiol., C* **2005**, *4*, 145−153.
(4) (a) Yu, G.; Gao, J.; Hummelen, J. C.; Wudl, F.; Heeger, A. J. *Science* **1995**, *270*, 1789−1791. (b) Halls, J. J. M.; Walsh, C. A.; Greenham, N. C.; Marseglia, E. A.; Friend, R. H.; Moratti, S. C.; Holmes, A. B. *Nature* **1995**, *376*, 498−500. (c) Peumans, P.; Yakimov, A.; Forrest, S. R. *J. Appl. Phys.* **2003**, *93*, 3693−3723.
(5) (a) Sadamoto, R.; Tomioka, N.; Aida, T. *J. Am. Chem. Soc.* **1996**, *118*, 3978−3979. (b) Kuciauskas, D.; Liddell, P. A.; Lin, S.; Johnson, T. E.; Weghorn, S. J.; Lindsey, J. S.; Moore, A. L.; Moore, T. A.; Gust, D. *J. Am. Chem. Soc.* **1999**, *121*, 8604−8614. (c) Choi, M.-S.; Aida, T.; Luo, H.; Araki, Y.; Ito, O.; *Angew. Chem., Int. Ed.* **2003**, *42*, 4060−4063. (d) Imahori, H.; Sekiguchi, Y.; Kashiwagi, Y.; Sato, T.; Araki, Y.; Ito, O.; Yamada, H.; Fukuzumi, S. *Eur. Chem. J.* **2004**, *10*, 3184−3196. (e) Jiang, D.-L.; Choi, C.-K.; Honda, K.; Li, W.-S.; Yuzawa, T.; Aida, T. *J. Am. Chem. Soc. Chem.* **2004**, *126*, 12084−12089.

Scheme 1. Molecular Structures of Zinc Complexes of Multiporphyrin Dendrimers DP_m (m = 6, 12, and 24), Fullerene-Appended Bipyridine Ligands Py_2F_n (n = 1−3), and Reference Compounds P_1 and Py_2, and Schematic Representation of the Complexation of DP_{24} with Py_2F_3

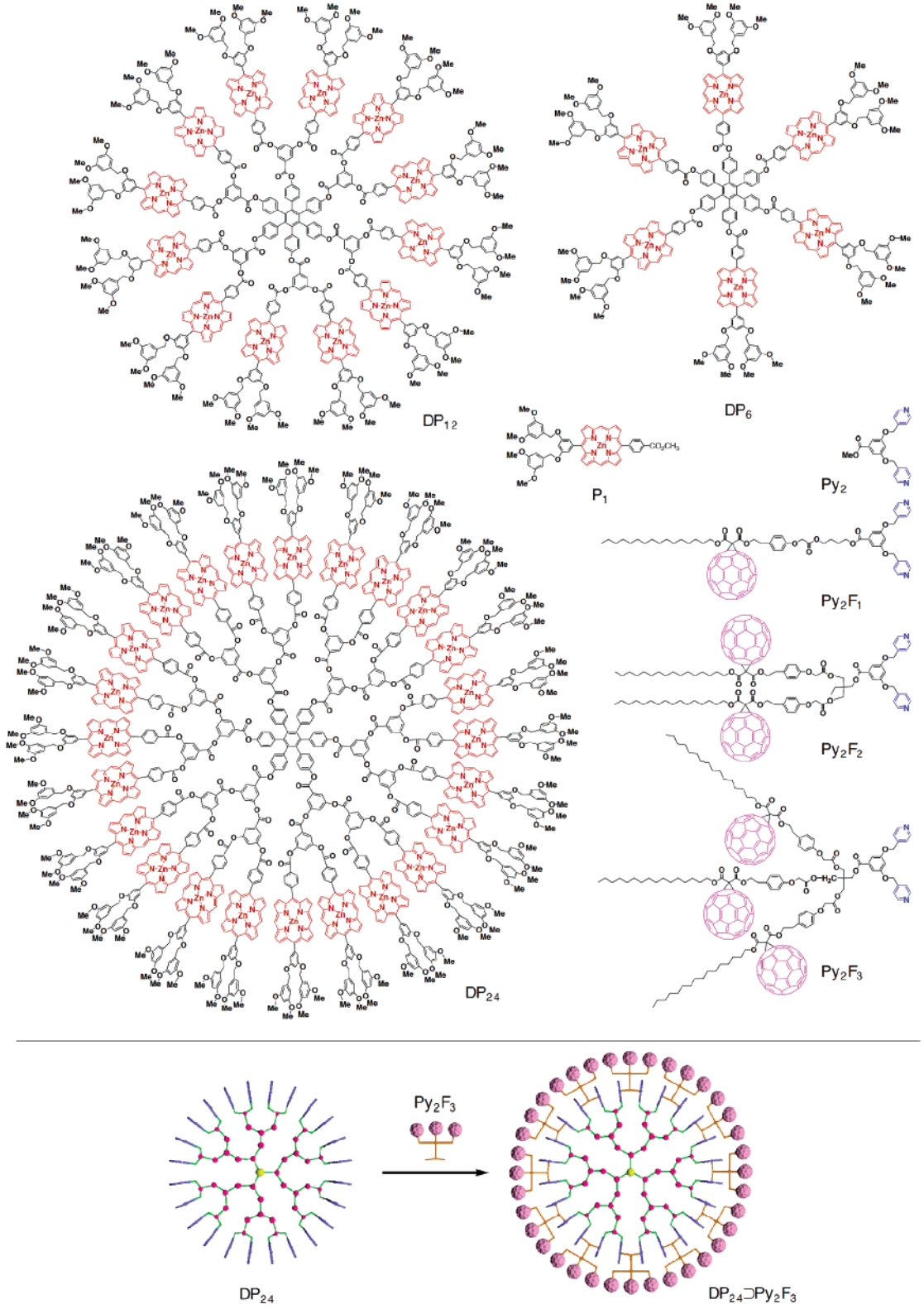

bipyridine and fullerene units in Py_2F_n are apart by roughly 2−3 nm from one another, the coordination of Py_2F_n to DP_m is expected to form a photoactive layer consisting of spatially segregated arrays of multiple donor (zinc porphyrin) and acceptor (fullerene) units on the dendrimer surface. Molecular design of DP_m was inspired by the unique structures of light-harvesting antenna complexes such as LH1 and LH2 in purple bacteria,[8] where multiple bacteriochlorophyll units are spatially arranged like a wheel and ensure efficient harvesting of dilute photons. The excitation energy captured by one of the bacteriochlorophyll unit migrates, without dissipation, to neighboring chlorophyll units in the same and connecting wheel-like chromophore arrays and is subsequently funneled to the photosynthetic reaction center, thereby triggering an electron

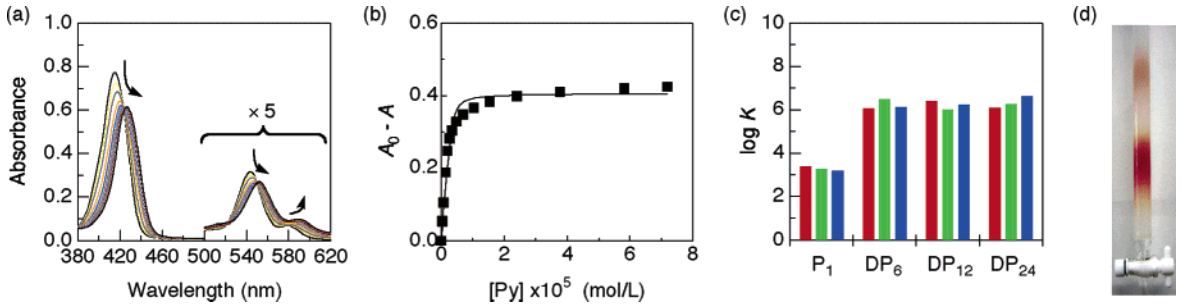

Figure 1. (a) Absorption spectral change of DP_{24} (1.5×10^{-7} M) upon titration with Py_2F_3 ([Py_2F_3]/[DP_{24}] = 0, 1.1, 2.3, 4.6, 6.8, 9.1, 11, 16, 23, 34, 52, 80, 126, 194, and 240) in $CHCl_3$ at 25 °C. (b) Change in absorbance ($A_0 - A$) of DP_{24}, monitored at 415.0 nm, as a function of [Py] (=2 × [Py_2F_3]), and its fitting profile. (c) Binding affinities (log K) of the pyridine units in Py_2F_1 (red), Py_2F_2 (green), and Py_2F_3 (blue) toward the zinc porphyrin units in P_1, DP_6, DP_{12}, and DP_{24} in $CHCl_3$ at 25 °C. (d) A snapshot of gel permeation chromatography (GPC) of a mixture of DP_{24} and Py_2F_3 ([Py_2F_3]/[DP_{24}] = 25) with $CHCl_3$ as an eluent.

transfer. We and other groups have reported that some dendritic multiporphyrin arrays including DP_m, upon photoexcitation, display highly efficient energy migration characteristics analogous to those of the biological light-harvesting systems.[6a,9] Hence, we decided to make use of zinc complexes of multiporphyrin dendrimers DP_m with a certain structural rigidity for an attempt to construct a concentric double layer of spatially segregated arrays composed of multiple D and A units (Scheme 1). As an electron acceptor for DP_m, we chose a fullerene such as C_{60} because of its small reorganization energy and excellent electron-accepting properties.[10] Thus, we synthesized Py_2F_n having 1−3 fullerene units (n = 1−3), where the bipyridine (Py_2) unit was expected to coordinate strongly in a bidentate fashion to two neighboring zinc porphyrin units in DP_m, thereby allowing the formation of a fullerene array outside of the zinc porphyrin array on the dendrimer surface ($DP_m \supset Py_2F_n$). Here, one can change the packing densities of these D and A units in the photoactive layer by varying the m and n values in the DP_m and Py_2F_n components, respectively, and might therefore be able to modulate the photoinduced charge-separation event.

Results and Discussion

Zinc complexes of multiporphyrin dendrimers DP_m (m = 6, 12, and 24) were synthesized according to a method analogous to that reported previously for chiroptical sensing of chiral bipyridine compounds.[7] On the other hand, fullerene-appended bipyridine ligands Py_2F_n (n = 1−3) were synthesized by coupling of a fullerene-containing carboxylic acid precursor with bipyridine-terminated alcohols bearing 1−3 hydroxyl groups.[11] In $CHCl_3$, DP_6 showed an absorption spectral profile typical of 5,15-diarylporphyrin zinc complexes, having a Soret absorption band centered at 414 nm and Q-bands at 542 and 578 nm. Compared with DP_6, DP_{24} showed a broad Soret absorption band centered at 415 nm, while DP_{12} showed a blue-shifted shoulder at 398 nm along with a major Soret band at 411 nm. The latter observation suggests that DP_{12} may adopt a planar geometry with a H-aggregate-type arrangement of the zinc porphyrin units along its periphery.[7] On the other hand, Py_2F_1−Py_2F_3 all displayed an electronic absorption band centered at 326 nm.[11] Upon excitation at 326 nm, all Py_2F_n fluoresced at 694 nm from their fullerene units.[10,11]

As expected, DP_m (m = 6, 12, and 24) bound Py_2F_n (n = 1−3) strongly to form stable $DP_m \supset Py_2F_n$. For example, upon titration with Py_2F_3 in $CHCl_3$ at 25 °C, DP_{24} (1.5×10^{-7} M) displayed a large spectral change in the Soret and Q-bands (Figure 1a), characteristic of the axial coordination of zinc porphyrins, with a clear saturation profile at a molar ratio [Py_2F_3]/[DP_{24}] exceeding 12 (Figure 1b). This spectral change profile did not give distinct isosbestic points possibly due to a large effect of the multivalency of the complexation between DP_{24} and Py_2F_3. However, the average binding affinity (K), as estimated by simply assuming a one-to-one coordination between the individual zinc porphyrin and pyridine units, was 1.2×10^6 M^{-1}.[11] This value is more than 2 orders of magnitude greater than association constants reported for monodentate coordination between zinc porphyrins and pyridine derivatives.[12] Other combinations of DP_m and Py_2F_n for the titration all showed analogous spectral change profiles with a marked saturation tendency at a mole ratio [Py_2F_n]/[DP_m] close to m/2.[11] Figure 1c shows average binding affinities K between the zinc porphyrin and pyridine units, which are almost comparable to one another in a range 1.1×10^6−4.4×10^6 M^{-1} irrespective of the m and n values in DP_m and Py_2F_n, respectively. We also found that resulting complexes $DP_m \supset Py_2F_n$ are all stable under conditions for gel permeation chromatography (GPC). For example, a $CHCl_3$ solution (0.5 mL) of a mixture of DP_{24} and Py_2F_3 ([DP_{24}] = 1.6×10^{-5} M, [Py_2F_3]/[DP_{24}] = 25) was loaded onto a Bio-beads S-X1 GPC column and then eluted with $CHCl_3$. As shown in Figure 1d, the chromatographic profile

(6) For dendritic multiporphyrin arrays: (a) Yeow, E. K. L.; Ghiggino, K. P.; Reek, J. N. H.; Crossley, M. J.; Bosman, A. W.; Schenning, A. P. H. J.; Meijer, E. W. *J. Phys. Chem. B* **2000**, *104*, 2596−2606. (b) Choi, M.-S.; Aida, T.; Yamazaki, T.; Yamazaki, I. *Angew. Chem., Int. Ed.* **2001**, *40*, 3194−3198. (c) Choi, M.-S.; Aida, T.; Yamazaki, T.; Yamazaki, I. *Chem. Eur. J.* **2002**, *8*, 2667−2678. (d) Benites, M. R.; et al. *J. Mater. Chem.* **2002**, *12*, 65−80. (e) Choi, M.-S.; Yamazaki, T.; Yamazaki, I.; Aida, T. *Angew. Chem., Int. Ed.* **2004**, *43*, 150−158. (f) Imahori, H. *J. Phys. Chem. B* **2004**, *108*, 6130−6143. (g) Solladié, N., Sooambar, C., Herschbach, H., Strub, J.-M., Leize, E., Van Dorsselaer, A., Talarico, A. M., Ventura, B., Flamigni, L. *New J. Chem.* **2005**, *29*, 1504−1507.

(7) Li, W.-S.; Jiang, D.-L.; Suna, Y.; Aida, T. *J. Am. Chem. Soc.* **2005**, *127*, 7700−7702.

(8) (a) Mcdermott, G.; Prince, S. M.; Freer, A. A.; Hawthornthwaite-Lawless, A. M.; Papiz, M. Z.; Cogdell, R. J.; Isaacs, N. W. *Nature* **1995**, *374*, 517−521. (b) Karrasch, S.; Bullough, P. A.; Ghosh, R. *EMBO J.* **1995**, *14*, 631−638. (c) Pullerits, T.; Sundström, V. *Acc. Chem. Res.* **1996**, *29*, 381−389.

(9) (a) Cho, S.; Li, W.-S.; Yoon, M.-C.; Ahn, T. K.; Jiang, D.-L.; Kim, J.; Aida, T.; Kim, D. *Chem. Eur. J.*, in press. (b) Fujitsuka, M.; Hara, M.; Tojo, S.; Okada, A.; Troiani, V.; Solladié, N.; Majima, T. *J. Phys. Chem. B* **2005**, *109*, 33−35.

(10) (a) Guldi, D. M.; Prato, M. *Acc. Chem. Res.* **2000**, *33*, 695−703. (b) Guldi, D. M. *Chem. Commun.* **2000**, 321−327. (c) Thomas, K. G.; George, M. V. *Helv. Chim. Acta* **2005**, *88*, 1291−1308.

(11) See Supporting Information.

(12) Sanders, J. K. M.; Bampos, N.; Clyde-Watson, Z.; Darling, S. L.; Hawley, J. C.; Kim, H.-J.; Mak, C. C.; Webb, S. J. In *Axial Coordination Chemistry of Metalloporphyrins*; Kadish, K. M., Smith, K. M., Guilard, R., Eds.; The Porphyrin Handbook; Academic Press: San Diego, 2000; Vol. 3, p 30.

Table 1. Average Numbers of Py_2F_n Bound to Single DP_m Molecule in $DP_m \supset Py_2F_n$, upon Mixing DP_m with Py_2F_n ($[Py_2F_n]/[DP_m] = m$) in $CHCl_3$ at 25 °C, Followed by GPC Separation with $CHCl_3$ as an Eluent (Figure 1d)[11]

	Py_2F_1	Py_2F_2	Py_2F_3
DP_6	2.9	2.6	2.6
DP_{12}	5.3	5.5	5.3
DP_{24}	9.0	9.6	9.5

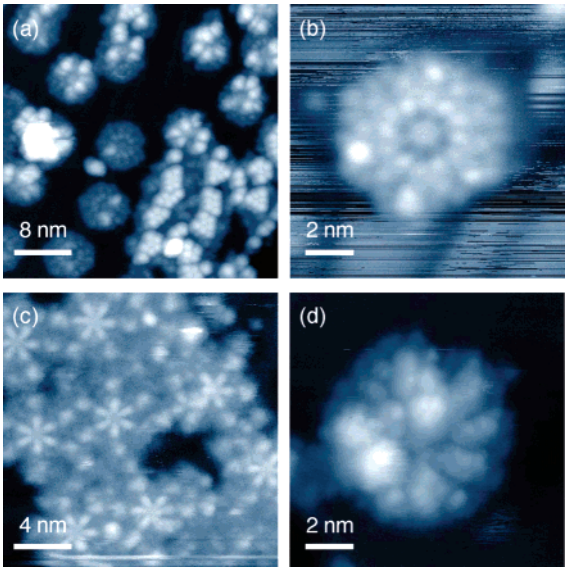

Figure 2. UHV−STM micrographs of (a, b) DP_{12} in the presence of 6 equiv of Py_2F_3, (c) DP_6 in the presence of 3 equiv of Py_2F_1, and (d) DP_{24} in the presence of 12 equiv of Py_2F_1, on a Au(111) surface at a liquid nitrogen temperature. Conditions: (a) $I = 1$ pA, $Vs = +3$ V; (b) $I = 1$ pA, $Vs = +2$ V; (c) $I = 2$ pA, $Vs = +4.5$ V; (d) I = 1 pA, $Vs = +2$ V.

displayed two colored fractions. By means of absorption spectroscopy, the first fraction was found to contain both DP_{24} and Py_2F_3 at a molar ratio $[Py_2F_3]/[DP_{24}]$ of 9.5 (Table 1), whereas the second fraction included Py_2F_3 alone.[11] The observed ratio of $[Py_2F_3]/[DP_{24}]$ is fairly close to an expected ratio of 12 for the bidentate ligation of Py_2F_3 to the zinc porphyrin units in DP_{24}. As summarized in Table 1, we likewise isolated by GPC $DP_m \supset Py_2F_n$ formed from the other combinations of DP_m and Py_2F_n and confirmed from their compositions that almost all the zinc porphyrin units in DP_m participate in the bidentate ligation with Py_2F_n. In contrast, P_1, a nondendritic zinc porphyrin reference (Scheme 1), incapable of bidentate ligation with Py_2F_n, exhibited much smaller binding affinities ($\sim 2.0 \times 10^3$ M^{-1}) toward $Py_2F_1-Py_2F_3$ (Figure 1c).

We succeeded in visualizing some of the coordination complexes between DP_m and Py_2F_n by scanning tunneling microscopy under ultrahigh vacuum conditions (UHV−STM). For example, when a $CHCl_3$ solution of a mixture of DP_{12} and Py_2F_3 ($[DP_{12}] = 2.0 \times 10^{-6}$, $[Py_2F_3]/[DP_{12}] = 8.2$) was deposited on a Au(111) surface by pulse injection,[13] UHV−STM at a liquid nitrogen temperature displayed petal-like patterns with a uniform diameter of 7 nm, assignable to DP_{12} adopting a planer conformation on the substrate surface (Figures 2a and 2b). UHV−STM also exhibited many bright spots at the periphery of DP_{12} molecules, which are most likely fullerene clusters of Py_2F_3. While $DP_6 \supset Py_2F_1$ showed a petal-like pattern

(13) (a) Tanaka, H.; Kawai, T. *J. Vac. Sci. Technol. B* **1997**, *15*, 602−604. (b) Tanaka, H.; Kawai, T. *Surf. Sci.* **2003**, *539*, L531−L536.

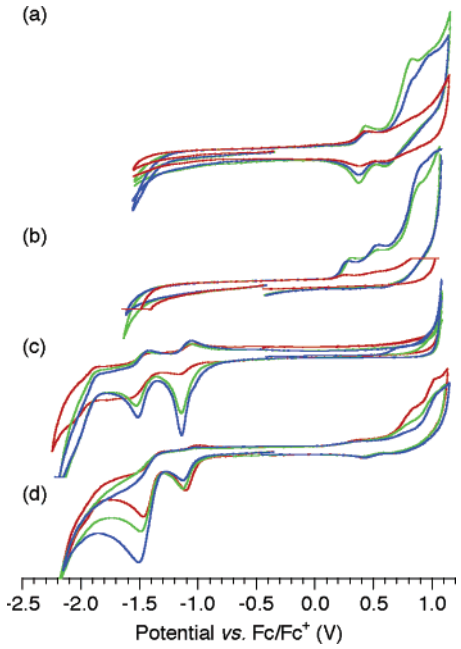

Figure 3. Cyclic voltammograms of (a) DP_6 (green), DP_{12} (blue), and DP_{24} (red) alone, (b) those in the presence of Py_2 ([pyridine]/[zinc porphyrin] = 1), (c) Py_2F_1 (red), Py_2F_2 (green), and Py_2F_3 (blue) alone, and (d) those in the presence of DP_{12} ([pyridine]/[zinc porphyrin] = 1). Conditions: 0.1 M $Bu_4N^+PF_6^-$ as a supporting electrolyte, scan rate: 100 mV/s, Pt electrodes, in CH_2Cl_2 at 25 °C.

(Figure 2c), the complex likely lost most of the ligating Py_2F_1 molecules during the process for pulse injection. On the other hand, as shown in Figure 2d, $DP_{24} \supset Py_2F_1$ in UHV−STM developed a rather obscure molecular image, possibly due to a difficulty of large DP_{24} in flattening on the substrate surface.

Electrochemical properties of DP_m, Py_2F_n, and reference complexes for $DP_m \supset Py_2F_n$ were investigated by means of cyclic voltammetry (CV). In CH_2Cl_2 at 25 °C, DP_6, DP_{12}, and DP_{24} displayed nearly identical redox properties to one another with the first oxidation potential ($E_{Ox}^{0/\cdot+}$) at around 0.40 V versus Fc/Fc^+ (Figure 3a). For the evaluation of the redox potentials of the pyridine-ligating zinc porphyrin units in $DP_m \supset Py_2F_n$, we utilized, in place of Py_2F_n, reference bipyridine compound Py_2 without fullerene units (Scheme 1). Upon addition of 3 equiv of Py_2 to a CH_2Cl_2 solution of DP_6, the oxidation peak, as expected, showed a cathodic shift down to $E_{Ox}^{0/\cdot+}$ of 0.28 V due to an electron donation from ligating Py_2 to the zinc porphyrin units (Figure 3b). A similar electronic effect of Py_2 was observed for the oxidation potentials of DP_{12} and DP_{24}, although the extent of such a cathodic shift was a little more explicit as the steric congestion of the dendrimer became larger: $E_{Ox}^{0/\cdot+} = 0.26$ (DP_{12}) and 0.23 V (DP_{24}). On the other hand, Py_2F_n showed the first reduction potential ($E_{Red}^{0/\cdot-}$) at −1.08 ($n = 1$), −1.10 ($n = 2$), and −1.10 ($n = 3$) versus Fc/Fc^+ in CH_2Cl_2 (Figure 3c), which remained virtually intact upon complexation with DP_m such as DP_{12} (Figure 3d).

Photoinduced electron transfer in $DP_m \supset Py_2F_n$ was confirmed by means of steady-state emission spectroscopy and nanosecond flash photolysis measurements. For example, excitation of a $CHCl_3$ solution of DP_{24} (1.5×10^{-7} M) at 550 nm resulted in a fluorescence emission from the zinc porphyrin units at 591 and 635 nm (Figure 4a). Upon titration with Py_2F_3, the fluorescence stepwise decreased in intensity and was quenched almost completely in the final stage. Stern−Volmer constants

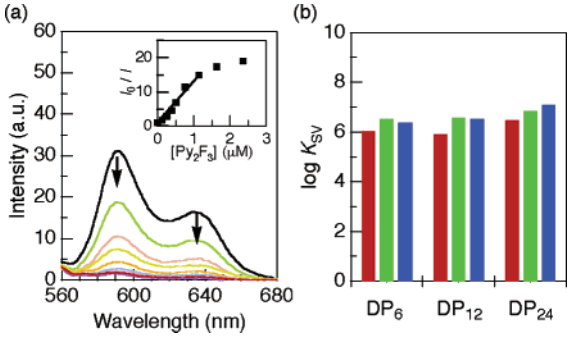

Figure 4. (a) Fluorescence spectral change and Stern−Volmer plot (inset) of DP_{24} (1.5×10^{-7} M) upon excitation at 550 nm in the presence of Py_2F_3 ([Py_2F_3]/[DP_{24}] = 0, 0.85, 1.7, 2.6, 3.4, 5.1, 7.7, 11, and 16 in $CHCl_3$ at 25 °C under Ar. (b) Stern−Volmer constants of DP_6, DP_{12}, and DP_{24} in the presence of Py_2F_1 (red), Py_2F_2 (green), and Py_2F_3 (blue).

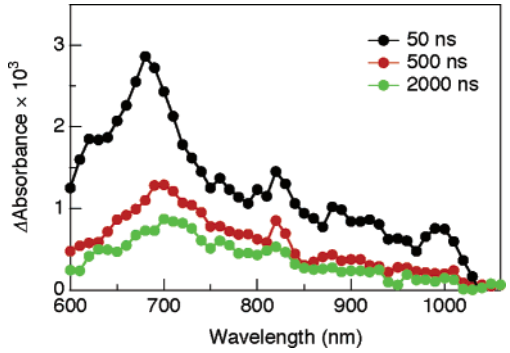

Figure 5. Nanosecond transient absorption spectra at 20 °C of a CH_2Cl_2 solution of DP_6 (1.7×10^{-5} M) containing 3 equiv of Py_2F_3 upon photoexcitation at 532 nm.

(K_{SV}, Figure 4b),[11] evaluated for the combination of DP_m (m = 6, 12, and 24) and Py_2F_n (n = 1−3), were roughly comparable to their average binding affinities K (Figure 1c), indicating that the fluorescence quenching of DP_m is caused by the coordination of electron-accepting Py_2F_n. By means of transient absorption spectroscopy, we confirmed the occurrence of an electron transfer from the photoexcited zinc porphyrin units in DP_m to the fullerene units in ligating Py_2F_n. Excitation of a CH_2Cl_2 solution of DP_6 (1.7×10^{-5} M) at 532 nm in the presence of 3 equiv of Py_2F_3 resulted in a transient absorption spectrum (Figure 5) with bands at around 680 and 1000 nm assignable to the cation and anion radicals of the zinc porphyrin and fullerene units, respectively. Broad absorption bands, observed at 750−900 nm, are due to the excited triplet states of these two units. Since the fluorescence spectral profiles of $DP_m \supset Py_2F_n$ such as $DP_6 \supset Py_2F_3$ under the conditions employed here did not show any sign of energy transfer from the photoexcited zinc porphyrin units in DP_m to the fullerene units of Py_2F_n,[11,14] we conclude that the quenching of the zinc porphyrin fluorescence observed for $DP_m \supset Py_2F_n$ (Figure 4) is mostly due to the intracomplex photoinduced electron transfer between them.

Time-resolved emission spectroscopy was employed for investigating the charge-separation event in $DP_m \supset Py_2F_n$.[11] Upon excitation at 420 nm in CH_2Cl_2 at 20 °C, the fluorescence of DP_6 (1.0×10^{-6} M) in the presence of 3 equiv of fullerene-free bipyridine displayed a monoexponential decay profile at 590 nm with a lifetime (τ_f) of 1.6 ns. On the other hand, when

(14) Kuciauskas, D.; Lin, S.; Seely, G. R.; Moore, A. L.; Moore, T. A.; Gust, D.; Drovetskaya, T.; Reed, C. A.; Boyd, P. D. W. *J. Phys. Chem.* **1996**, *100*, 15926−15932.

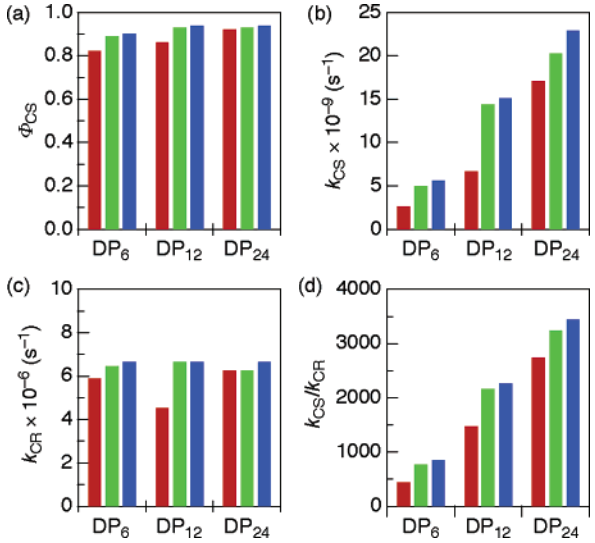

Figure 6. (a) Charge-separation quantum yields (Φ_{CS}), (b) charge-separation rate constants (k_{CS}), (c) charge-recombination rate constants (k_{CR}), and (d) k_{CS}/k_{CR} of DP_6, DP_{12}, and DP_{24} in the presence of Py_2F_1 (red), Py_2F_2 (green), and Py_2F_3 (blue) in CH_2Cl_2 at 20 °C.

fullerene-appended Py_2F_1 was used in place of Py_2, a fast-decay fluorescing component with τ_f of 320 ps appeared in addition to the slow-decay component (τ_f = 1.1 ns). This fast-decay component obviously originates from the charge-separation process caused by the photoinduced electron transfer from DP_6 to Py_2F_1. In the presence of Py_2F_2 or Py_2F_3 instead of Py_2F_1, the lifetime of the fast-decay component of DP_6 became much shorter; τ_f = 170 (Py_2F_2) and 150 ps (Py_2F_3). In contrast with $DP_6 \supset Py_2$, $DP_{12} \supset Py_2$ and $DP_{24} \supset Py_2$ exhibited a biexponential fluorescence decay at 590 nm possibly due to a dense packing of the zinc porphyrin units (vide ante) on the dendrimer surface.[11] Use of Py_2F_n in place of Py_2 to allow complexation with DP_{12} or DP_{24} resulted in an additional decay component with a much shorter τ_f value, owing to the electron transfer from DP_m to Py_2F_n.[11] On the basis of the fluorescence decay profiles, the charge-separation rate constants (k_{CS}) and quantum yields (Φ_{CS}) were evaluated according to the following equations by comparison of the shortest τ_f components of $DP_m \supset Py_2F_n$ with average τ_f values of $DP_m \supset Py_2$:

$$k_{CS} = \left(\frac{1}{\tau_f}\right)_{DP_m \supset Py_2F_n} - \left(\frac{1}{\tau_f}\right)_{DP_m \supset Py_2}$$

$$\Phi_{CS} = \left[\left(\frac{1}{\tau_f}\right)_{DP_m \supset Py_2F_n} - \left(\frac{1}{\tau_f}\right)_{DP_m \supset Py_2}\right] \Big/ \left(\frac{1}{\tau_f}\right)_{DP_m \supset Py_2F_n}$$

The Φ_{CS} values thus evaluated are all high, ranging from 0.82 to 0.94 (Figure 6a). Thus, the photoinduced electron transfer in $DP_m \supset Py_2F_n$ occurred very efficiently, irrespective of the magnitudes of m and n. Of further interest, the k_{CS} value increases following the order of $Py_2F_1 < Py_2F_2 < Py_2F_3$ and enhances, to a much greater extent, from DP_6 to DP_{12} and then to DP_{24} (Figure 6b). For example, the k_{CS} value of 2.3×10^{10} s^{-1}, as evaluated for $DP_{24} \supset Py_2F_3$, is an order of magnitude greater than that of $DP_6 \supset Py_2F_1$ (0.26×10^{10} s^{-1}) and obviously the largest among those of the $DP_m \supset Py_2F_n$ family. These trends indicate an interesting possibility that dense packing of both the zinc porphyrin and fullerene units on the dendrimer surface

plays an essential role in facilitating the charge-separation process. As expected, nondendritic zinc porphyrin reference P_1 in the presence of Py_2F_n showed much smaller k_{CS} values such as 0.031×10^{10} ($n = 1$), 0.12×10^{10} ($n = 2$), and 0.13×10^{10} s^{-1} ($n = 3$).

We also investigated the charge-recombination events in $DP_m \supset Py_2F_n$, using the decay profiles in CH_2Cl_2 of the transient absorption band at 1000 nm due to $C_{60}^{\bullet -}$ (Figure 5).[11] In every case, the decay profile was satisfactorily fitted with two-exponential components, where the faster decay is attributed to the charge-recombination process, while the slower decay originates from the excited triplet species. The charge-recombination rate constants (k_{CR}, Figure 6c) thus obtained are all within a narrow range from 4.5×10^6 to 6.7×10^6 s^{-1}, and the lifetimes of the charge-separation state (τ_{RIP}; 150−220 ns) are comparable to one another.[11] These trends are quite reasonable since the donor−acceptor distance in $DP_m \supset Py_2F_n$ should not be much dependent on the degrees of steric congestion of the two ligating components but is primarily determined by the length of the spacer unit between the bipyridine and fullerene units in Py_2F_n. The successful determination of the k_{CS} values for $DP_m \supset Py_2F_n$ allowed us to compare the ratios of k_{CS}/k_{CR}, which have often been used as a measure for the excellence of photoinduced electron-transfer systems.[15] Of interest, the values of k_{CS}/k_{CR} (Figure 6d) are all large in a range from 450 ($DP_6 \supset Py_2F_1$) to 3400 ($DP_{24} \supset Py_2F_3$). In particular, the k_{CS}/k_{CR} ratio for $DP_{24} \supset Py_2F_3$ is more than an order of magnitude greater than those reported for precedent porphyrin−fullerene supramolecular dyads and triads.[15] It is obvious that a larger number of the fullerene units in $DP_{24} \supset Py_2F_3$ could enhance the probability of the electron transfer from the zinc porphyrin units. However, in addition to this, one can also presume that an efficient energy migration along the densely packed zinc porphyrin array[9] may enhance the opportunity for this electron transfer. When the degrees of fluorescence quenching ($1 - I/I_0$) [I and I_0; fluorescence intensities with and without the quencher, respectively], observed for DP_6, DP_{12}, and DP_{24} upon titration with Py_2F_3, are plotted against the ratio of the numbers of the fullerene and zinc porphyrin units ([fullerene]/[zinc porphyrin]),[11] it is clear that the quenching of the excited singlet state of the zinc porphyrin units by Py_2F_3 is more efficient as m in DP_m is larger from 6 to 12 and then to 24 (Figure 7). For example, the degree of fluorescence quenching of 0.6 can be attained for DP_{24} only at [fullerene]/[zinc porphyrin] = 0.19, whereas it requires a much larger ratio of [fullerene]/[zinc porphyrin] such as 0.64 for DP_6. Since the average binding affinities of Py_2F_3 toward DP_6 and DP_{24} are not much different from one another (Figure 1c), it is obvious that the energy migration along the zinc porphyrin array in DP_{24}[9] greatly facilitates the electron transfer to the fullerene units.

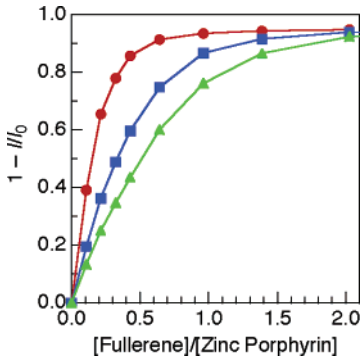

Figure 7. Plots of degrees of fluorescence quenching ($1 - I/I_0$) versus [fullerene]/[zinc porphyrin] upon titration of DP_6 (green), DP_{12} (blue), and DP_{24} (red) ([zinc porphyrin] = 3.6×10^{-6} M) with Py_2F_3 in $CHCl_3$ at 25 °C. Concentrations of fullerene and zinc porphyrin units are given by $3 \times$ [Py_2F_3] and $m \times$ [DP_m], respectively.

Conclusions

By means of a multivalent surface ligation of dendritic macromolecules,[16] we constructed, using DP_m ($m = 6$, 12, and 24) and Py_2F_n ($n = 1-3$), a photoactive layer, consisting of electron-donating zinc porphyrin and electron-accepting fullerene arrays on the dendrimer surface. Upon increment of the numbers of these donor and acceptor units, the electron transfer reaction was remarkably facilitated, while the recombination of the resulting charge-separated state remained virtually intact. Consequently, among the $DP_m \supset Py_2F_n$ family, $DP_{24} \supset Py_2F_3$ accommodating 24 zinc porphyrin units and roughly 30 fullerene units on the dendrimer surface (Table 1) achieved the largest ratio of the charge-separation to charge-recombination rate constants (3400), which is even 1 order of magnitude greater than those of precedent examples. Application of this molecular design strategy to the development of optoelectronic materials is one of the subjects worthy of further investigations.

Acknowledgment. We are grateful to Dr. Yohei Yamamoto for STM measurements. D.K. acknowledges the financial support through the Star Faculty Program of the Ministry of Education and Human Resources.

Supporting Information Available: Details for synthesis, characterization, and spectral data (PDF). This material is available free of charge via the Internet at http://pubs.acs.org. See any current masthead page for ordering information and Web access instructions.

JA063081T

(15) (a) D'Souza, F.; Gadde, S.; Zandler, M. E.; Arkady, K.; El-Khouly, M. E.; Fujitsuka, M.; Ito, O. *J. Phys. Chem. A* **2002**, *106*, 12393−12404. (b) D'Souza, F.; Deviprasad, G. R.; Zandler, M. E.; El-Khouly, M. E.; Fujitsuka, M.; Ito, O. *J. Phys. Chem. A* **2003**, *107*, 4801−4807. (c) D'Souza, F.; Smith, P. M.; Gadde, S.; McCarty, A. L.; Kullman, M. J.; Zandler, M. E.; Itou, M.; Araki, Y.; Ito, O. *J. Phys. Chem. B* **2004**, *108*, 11333−11343. (d) D'Souza, F.; El-Khously, M. E.; Gadde, S.; McCarty, A. L.; Karr, P. A.; Zandler, M. E.; Araki, Y.; Ito, O. *J. Phys. Chem. B* **2005**, *109*, 10107−10114.

(16) (a) Fréchet, J. M. J. *Proc. Acad. Sci., U.S.A.* **2002**, *99*, 4782−4787. (b) Broeren, M. A. C.; van Dongen, J. L. J.; Pitterlkow, M.; Christensen, J. B.; van Genderen, M. H. P.; Meijer, E. W. *Angew. Chem., Int. Ed.* **2004**, *43*, 3557−3562. (c) van Baal, I.; Malda, H.; Synowsky, S. A.; van Dongen, J. L. J.; Hackeng, T. M.; Merkx, M.; Meijer, E. W. *Angew. Chem., Int. Ed.* **2005**, *44*, 5052−5057. (d) Smith, D. K. *Chem. Commun.* **2006**, 34−44.

Supporting Information

Construction of Segregated Arrays of Multiple Donor and Acceptor Units Using a Dendritic Scaffold: Remarkable Dendrimer Effects on Photoinduced Charge Separation

Wei-Shi Li,[*,†] Kil Suk Kim,[§] Dong-Lin Jiang,[†] Hiroyuki Tanaka,[#]
Tomoji Kawai,[#] Jung Ho Kwon,[§] Dongho Kim,[*,§] and Takuzo Aida[*,†,‡]

[†]*ERATO-SORST Nanospace Project, Japan Science and Technology Agency (JST), 2-41 Aomi, Koto-ku, Tokyo 135-0064, Japan.*

[#]*The Institute of Scientific and Industrial Research (ISIR), Osaka University, 8-1, Mihogaoka, Ibaragi, Osaka 567-0047, Japan.*

[§]*National Creative Research Initiatives, Center for Ultrafast Optical Characteristics Control and Department of Chemistry, Yonsei University, Seoul 120-749, Korea.*

[‡]*Department of Chemistry and Biotechnology, School of Engineering, and Center for NanoBio Integration, The University of Tokyo, 7-3-1 Hongo, Bunkyo-ku, Tokyo 113-8656, Japan.*

Contents

1. Measurements and Methods

^{1}H NMR spectra were recorded on a JEOL model Excalibur-500 FT NMR spectrometer, where chemical shifts were determined with respect to non-deuterated residues of solvents as internal references. MALDI-TOF-MS spectra were recorded on an Applied Biosystems model BioSpectrometry Workstation™ Voyager-DE™ STR mass spectrometer using α-cyano-4-hydroxycinnamic acid (CHCA) or dithranol as a matrix in a reflector mode. Electronic absorption and fluorescence spectra were recorded in $CHCl_3$ at 25 °C using a quartz cell of 1-cm path length on a JASCO model V-570 spectrophotometer and a JASCO model FP-6500 spectrofluorometer, respectively. Recycling preparative SEC was performed with THF or $CHCl_3$ as an eluent using JAIGEL 1H (pore size: 20–30 Å), 2H (40–50 Å), and/or 3H (> 50 Å) columns on a JAI model LC-908 recycling HPLC system equipped with a JASCO model MD-2010 variable-wavelength UV-vis detector. UHV-STM measurements were performed on a Unisoku model USM-1200S2N1 STM microscope. Samples were deposited on a Au(111) surface from their $CHCl_3$ solutions by pulse injection, reported previously.[1] Cyclic voltammetry (CV) was performed on an ALS/[H] CH Instruments model 619B electrochemical analyzer using platinum-wire working and counter electrodes and a silver-wire pseudo reference electrode. Sample solutions of DP_m ([zinc porphyrin] = 0.2 mM in CH_2Cl_2) and Py_2F_n ([fullerene] = 0.2 mM in CH_2Cl_2) containing Bu_4NPF_6 (0.1 M) as a supporting electrolyte were degassed by several freeze-pump-thaw cycles prior to measurements, where redox potentials were determined with respect to ferrocene as an internal standard.

Time-resolved fluorescence data were recorded using a time-correlated single-photon-counting (TCSPC) technique on a home-made system consisting of a home-made cavity dumped Ti:Sapphire oscillator pumped by a Coherent model Verdi CW Nd-YVO4 laser as the excitation light source, which provided ultrashort pulses with a full width half maximum (FWHM) of 100 fs and allowed for a high repetition rate (200–400 kHz). The output pulse of the oscillator was frequency-doubled with a second harmonic crystal. The TCSPC detection system consisted of a Hamamatsu model R3809U–51 multichannel plate photomultiplier equipped with a Hamamatsu model C4878 cooler, a EG&G Ortec model 457 time-to-amplitude converter (TAC), a EG&G Ortec model 584 signal discriminator, a Canberra model 2126 trigger discriminator, a Philip Scientific signal wideband amplifier, a Mini Circuit trigger wideband

[1] (a) Tanaka, H.; Kawai, T. *J. Vac. Sci. Technol. B* **1997**, *15*, 602–604. (b) Tanaka, H.; Kawai, T. *Surf. Sci.* **2003**, *539*, L531–L536.

amplifier and a computer equipped with a Canberra model PCA3 multichannel analyzer. The overall instrumental response function was about 60 ps (FWHM). A sheet polarizer, set at an angle complementary to the magic angle (54.7°), was placed in the fluorescence collection system. The decay profiles were fitted using a LIFETIME program with an iterative nonlinear least-squares deconvolution procedure developed at the University of Pennsylvania.

Nanosecond transient absorption spectra were measured using a nanosecond flash photolysis technique. Excitation pulses of 532 nm with a time duration of ca. 6 ns and energy of ca. 2 mJ/pulse were generated from the second harmonic output of a Continuum model Surelite Q-switched Nd:YAG laser. The probe light generated by a cw Xe lamp (150 W) was collimated on the sample cell and then spectrally resolved by using a Acton Research model SP150 monochromator (15 cm) equipped with a 600 grooves/mm grating with a spectral resolution of about 3 nm. The light signal was detected by using a Hamamatsu model C5331 Si avalanche photodiode, and recorded with a Tektronix model TDS3052 500 MHz digital storage oscilloscope. To ensure the data, we first examined the triplet state dynamics of zinc(II) tetraphenylporphyrin in toluene at 25 ºC, which gave the lifetime of 1 ms.

2. Synthesis

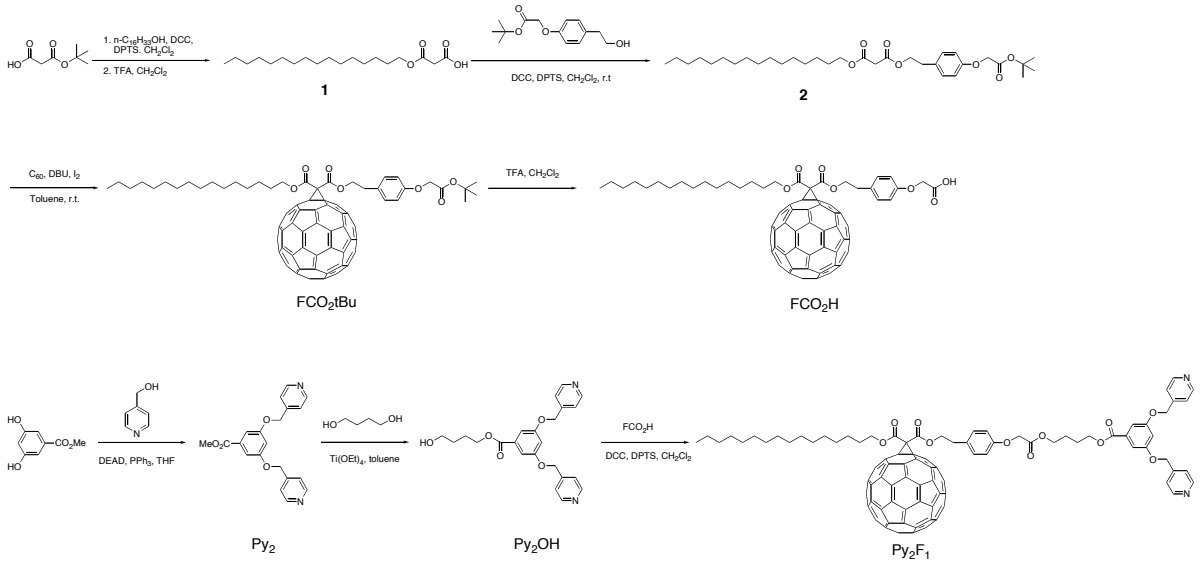

Scheme S1. Synthesis of Py_2F_1.

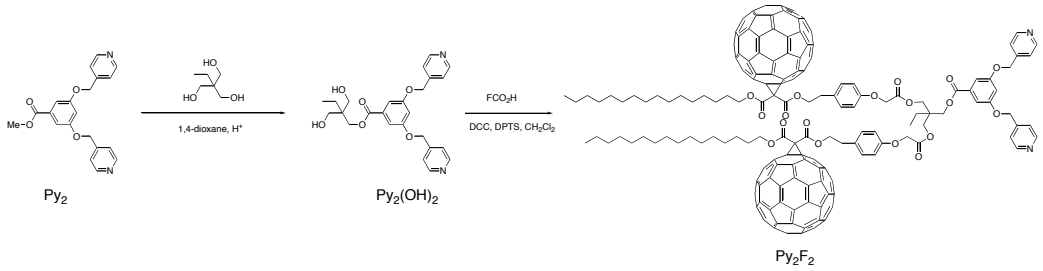

Scheme S2. Synthesis of Py_2F_2.

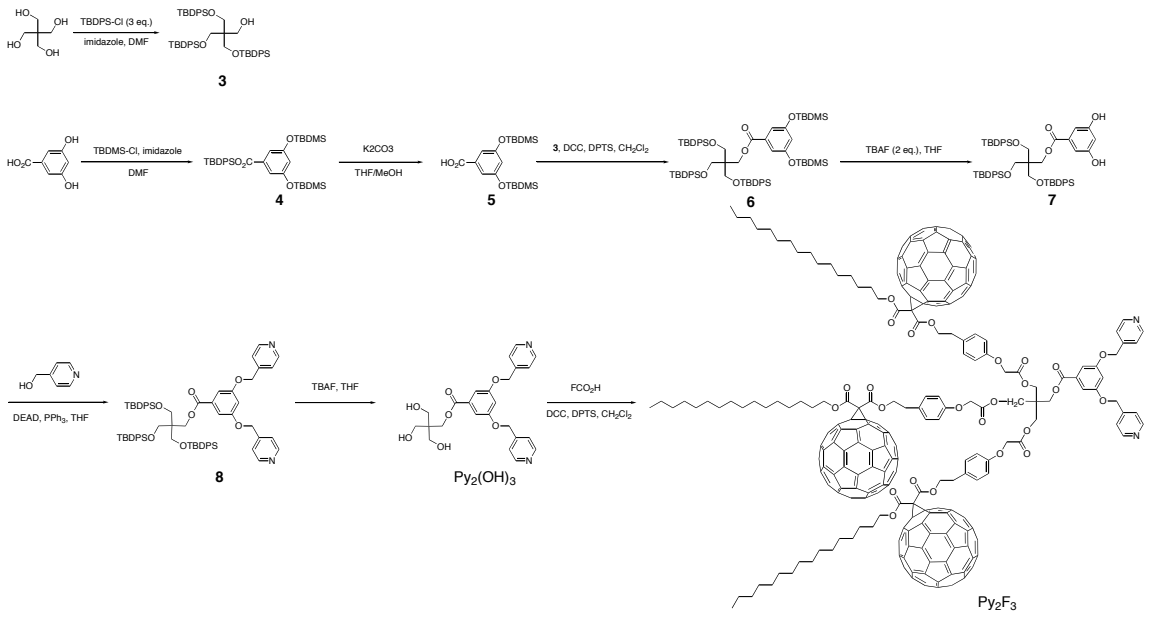

Scheme S3. Synthesis of Py_2F_3.

1. To a CH_2Cl_2 solution (20 mL) of a mixture of hexadecanol (3 g, 0.0124 mol), mono-*tert*-butylmalonate (2.17 g, 0.0135 mol), and 4-(dimethylamino)pyridinium 4-toluenesulfonate (DPTS)[2] (0.375 g, 1.27 mmol) was added a CH_2Cl_2 solution (20 mL) of dicyclohexylcarbodiimide (DCC) (3.94 g, 0.0191 mol), and the mixture was stirred at room temperature overnight. The reaction mixture was filtered off from an insoluble fraction, and the filtrate was concentrated and chromatographed on silica gel with CH_2Cl_2 as an eluent, where the first fraction was collected and evaporated to dryness. The residue was dissolved in TFA (5 mL) and stirred at room temperature. After 1 h, the reaction mixture was evaporated to dryness, and the residue was chromatographed on silica gel with $CHCl_3$/THF (0–5%; gradient) as an eluent, to allow isolation of **1** as a white powdery substance (3.46 g) in 85% yield. ^{1}H NMR (500 MHz, $CDCl_3$, 25 °C): δ (ppm) 4.18 (t, J = 7.0 Hz, 2H, $OCH_2CH_2(CH_2)_{13}CH_3$), 3.42 (s, 2H, $HOOCCH_2COO$), 1.65 (m, 2H, $OCH_2CH_2(CH_2)_{13}CH_3$), 1.33–1.21 (m, 26H, $OCH_2CH_2(CH_2)_{13}CH_3$), 0.86 (t, J = 7.0 Hz, 3H, $OCH_2CH_2(CH_2)_{13}CH_3$).

2. To a CH_2Cl_2 solution (10 mL) of a mixture of **1** (336 mg, 1.02 mmol), *tert*-butyl 2-[4-(2-hydroxyethyl)phenoxy]acetate (215 mg, 0.0135 mol), and DPTS (59 mg, 0.20 mmol) was added a CH_2Cl_2 solution (10 mL) of DCC (383 mg, 1.85 mmol), and the mixture was stirred at room temperature. After 1 day, the reaction mixture was extracted with hexane/MeOH/water, and the combined organic extract was dried over $MgSO_4$ and evaporated to dryness. The residue was subjected to recycling preparative SEC (1H/2H columns) with $CHCl_3$ as an eluent, to allow isolation of **2** as a white powdery substance (406 mg) in 85% yield. MS (MALDI-TOF, CHCA, reflector mode): m/z 585.28 ($[M + Na]^+$, calcd. for $C_{33}H_{54}O_7$: 562.78). ^{1}H NMR (500 MHz, $CDCl_3$, 25 °C): δ (ppm) 7.10 (d, J = 10.5 Hz, 2H, *m*-H of $CH_2C_6H_4O$), 6.81 (d, J = 10.5 Hz, 2H, *o*-H of $CH_2C_6H_4O$), 4.47 (s, 2H, $OCH_2CO_2{}^tBu$), 4.29 (t, J = 7.5 Hz, 2H, OCH_2CH_2Ar), 4.10 (t, J = 7.0 Hz, 2H, $OCH_2CH_2(CH_2)_{13}CH_3$), 3.33 (s, 2H, $OOCCH_2COO$), 2.87 (t, J = 7 Hz, 2H, OCH_2CH_2Ar), 1.61 (m, 2H, $OCH_2CH_2(CH_2)_{13}CH_3$), 1.47 (s, 9H, $OCH_2CO_2C(CH_3)_3$), 1.23 (m, 26H, $OCH_2CH_2(CH_2)_{13}CH_3$), 0.86 (t, J = 7.0 Hz, 3H, $OCH_2CH_2(CH_2)_{13}CH_3$).

FCO_2tBu. To a toluene solution (250 mL) of C_{60} (284 mg, 0.394 mmol) was added **2** (220 mg, 0.39 mmol), iodine (108 mg, 0.43 mmol), and 1,8-diazabicyclo[5,4,0]-7-undecene (DBU) (61 mg, 0.401 mmol), and the mixture was stirred at room temperature. After 7 h, the reaction mixture

[2] Moore, J. S.; Stupp, S. I. *Macromolecules* **1990**, *23*, 65–70.

was chromatographed on silica gel with toluene as an eluent, where the second fraction was collected and chromatographed on silica gel with $CHCl_3$ as an eluent, to allow isolation of FCO_2tBu as a dark brown powdery substance (294 mg) in 59% yield. MS (MALDI-TOF, dithranol, reflector mode): m/z 1280.85 (M^+, calcd. for $C_{93}H_{52}O_7$: 1281.35). ^1H NMR (500 MHz, $CDCl_3$, 25 °C): δ (ppm) 7.19 (d, J = 10.5 Hz, 2H, *m*-H of $CH_2C_6H_4O$), 6.81 (d, J = 10.5 Hz, 2H, *o*-H of $CH_2C_6H_4O$), 4.65 (t, J = 7.0 Hz, 2H, OCH_2CH_2Ar), 4.45 (s, 2H, $OCH_2CO_2{}^tBu$), 4.42 (t, J = 7.0 Hz, 2H, $OCH_2CH_2(CH_2)_{13}CH_3$), 3.08 (t, J = 7 Hz, 2H, OCH_2CH_2Ar), 1.77 (m, 2H, $OCH_2CH_2(CH_2)_{13}CH_3$), 1.47 (s, 9H, $OCH_2CO_2C(CH_3)_3$), 1.23 (m, 26H, $OCH_2CH_2(CH_2)_{13}CH_3$), 0.86 (t, J = 7.0 Hz, 3H, $OCH_2CH_2(CH_2)_{13}CH_3$).

FCO_2H. To a CH_2Cl_2 solution (5 mL) of FCO_2tBu (294 mg, 0.229 mmol) was added TFA (5 mL), and the mixture was stirred at room temperature. After 30 min, the reaction mixture was concentrated and chromatographed on silica gel with CH_2Cl_2/THF (0–5%; gradient) as an eluent, to allow isolation of FCO_2H (273 mg) as a dark brown powdery substance in 96% yield. MS (MALDI-TOF, dithranol, reflector mode): m/z 1223.87 (M^+, calcd. for $C_{89}H_{44}O_7$: 1225.24). ^1H NMR (500 MHz, $CDCl_3$, 25 °C): δ (ppm) 7.22 (d, J = 10.5 Hz, 2H, *m*-H of $CH_2C_6H_4O$), 6.84 (d, J = 10.5 Hz, 2H, *o*-H of $CH_2C_6H_4O$), 4.67 (t, J = 7.0 Hz, 2H, OCH_2CH_2Ar), 4.61 (s, 2H, OCH_2CO_2H), 4.42 (t, J = 7.0 Hz, 2H, $OCH_2CH_2(CH_2)_{13}CH_3$), 3.09 (t, J = 7 Hz, 2H, OCH_2CH_2Ar), 1.77 (m, 2H, $OCH_2CH_2(CH_2)_{13}CH_3$), 1.47 (s, 9H, $OCH_2CO_2C(CH_3)_3$), 1.23 (m, 26H, $OCH_2CH_2(CH_2)_{13}CH_3$), 0.86 (t, J = 7.0 Hz, 3H, $OCH_2CH_2(CH_2)_{13}CH_3$).

Py_2. To an ice-cooled THF solution (40 mL) of a mixture of methyl 3,5-dihydroxybenzoate (2 g, 11.89 mmol), 4-hydroxymethylpyridine (2.73 g, 25.13 mmol), and PPh_3 (6.55 g, 25.14 mmol) was dropwise added a toluene solution of diethyl azodicarboxylate (DEAD, 40 wt.%, 12 mL) under Ar, and the mixture was stirred at room temperature. After 2 days, the reaction mixture was evaporated to dryness, and the residue was chromatographed on silica gel with $CHCl_3$/MeOH (0–5%, gradient) as an eluent, where the third fraction was collected and evaporated to dryness, leaving Py_2 as a white powdery substance (3.62 g) in 87% yield. MS (MALDI-TOF, dithranol, reflector mode): m/z 350.88 (M^+, calcd. for $C_{20}H_{18}N_2O_4$: 350.37). ^1H NMR (500 MHz, $CDCl_3$, 25 °C): δ (ppm) 8.62 (d, J = 6.0 Hz, 4H, *o*-H of CH_2Py), 7.36 (d, J = 5.0 Hz, 4H, *m*-H of CH_2Py), 7.27 (d, J = 2.5 Hz, 2H, *o*-H of $(MeO_2C)C_6H_3(OCH_2Py)_2$), 6.77 (d, J = 2 Hz, 1H, *p*-H of $(MeO_2C)C_6H_3(OCH_2Py)_2$), 5.11 (s, 4H, $(MeO_2C)C_6H_3(OCH_2Py)_2$), 3.89 (s, 3H, CO_2CH_3).

Py_2OH. To a toluene solution (50 mL) of a mixture of Py_2 (1.51 g, 4.31 mmol) and 1,4-butanediol (10 mL) was added $Ti(OEt)_4$ (0.6 mL), and the mixture was refluxed under Ar in a flask equipped with a Dean-Stark trap. After the complete disappearance of Py_2 was confirmed by TLC, the reaction mixture was poured into water and extracted with CH_2Cl_2. The combined organic extract was dried over Na_2SO_4, concentrated, and chromatographed on silica gel with CH_2Cl_2/MeOH (0–5%, gradient) as an eluent, to allow isolation of Py_2OH as a white powdery substance (1.35 g) in 77% yield. MS (MALDI-TOF, dithranol, reflector mode): m/z 408.91 (M^+, calcd. for $C_{23}H_{24}N_2O_5$: 408.45). ^{1}H NMR (500 MHz, $CDCl_3$, 25 °C): δ (ppm) 8.48 (d, J = 5.0 Hz, 4H, *o*-H of CH_2*Py*), 7.23 (d, J = 4.5 Hz, 4H, *m*-H of CH_2*Py*), 7.15 (s, 2H, *o*-H of $(MeO_2C)C_6H_3(OCH_2Py)_2$), 6.66 (s, 1H, *p*-H of $(MeO_2C)C_6H_3(OCH_2Py)_2$), 4.98 (s, 4H, $(MeO_2C)C_6H_3(OCH_2Py)_2$), 4.22 (t, J = 6.5 Hz, 2H, $ArCO_2CH_2CH_2CH_2CH_2OH$), 3.95 (b, 1H, $ArCO_2CH_2CH_2CH_2CH_2OH$), 3.60 (t, J = 6.5 Hz, 2H, $ArCO_2CH_2CH_2CH_2CH_2OH$), 1.75 (m, 2H, $ArCO_2CH_2CH_2CH_2CH_2OH$), 1.59 (m, 2H, $ArCO_2CH_2CH_2CH_2CH_2OH$).

Py_2F_1. To a CH_2Cl_2 solution (5 mL) of a mixture of FCO_2H (166 mg, 0.135 mmol), Py_2OH (51.7 mg, 0.126 mol), and DPTS (24 mg, 0.08 mmol) was added a CH_2Cl_2 solution (6 mL) of DCC (44 mg, 0.215 mmol), and the mixture was stirred at room temperature. After 1 day, the reaction mixture was filtrated off from an insoluble fraction, and the filtrate was concentrated and subjected to recycling preparative SEC (1H/2H columns) with $CHCl_3$ as an eluent, where the first fraction was collected and subjected to preparative TLC (SiO_2) with CH_2Cl_2/MeOH (3%) as an eluent, affording pure Py_2F_1 as a dark brown powdery substance (158 mg) in 77% yield. MS (MALDI-TOF, dithranol, reflector mode): m/z 1616.05 ($[M + 1]^+$, calcd. for $C_{112}H_{66}N_2O_{11}$: 1615.68). ^{1}H NMR (500 MHz, $CDCl_3$, 25 °C): δ (ppm) 8.63 (br, 4H, *o*-H of CH_2*Py*), 7.42 (br, 4H, *m*-H of CH_2*Py*), 7.25 (d, J = 2.0 Hz, 2H, *o*-H of $(RO_2C)C_6H_3(OCH_2Py)_2$), 7.18 (d, J = 8.5 Hz, 2H, *m*-H of $CH_2C_6H_4O$), 6.79 (d, J = 10.5 Hz, 2H, *o*-H of $CH_2C_6H_4O$), 6.77 (br, 1H, *p*-H of $(RO_2C)C_6H_3(OCH_2Py)_2$), 5.13 (s, 4H, $(RO_2C)C_6H_3(OCH_2Py)_2$), 4.64 (t, J = 7.0 Hz, 2H, OCH_2CH_2Ar), 4.56 (s, 2H, $ArOCH_2CO_2R$), 4.42 (t, J = 6.5 Hz, 2H, $OCH_2CH_2(CH_2)_{13}CH_3$), 4.31 (br, 2H, $ArCO_2CH_2CH_2CH_2CH_2OCOCH_2OAr$), 4.27 (br, 2H, $ArCO_2CH_2CH_2CH_2CH_2OCOCH_2OAr$), 3.06 (t, J = 7 Hz, 2H, OCH_2CH_2Ar), 1.79 (m, 6H, $OCH_2CH_2CH_2(CH_2)_{12}CH_3$ and $ArCO_2CH_2CH_2CH_2CH_2OCOR$), 1.42 (m, 2H, $OCH_2CH_2CH_2(CH_2)_{12}CH_3$), 1.22 (m, 24H, $OCH_2CH_2CH_2(CH_2)_{12}CH_3$), 0.85 (t, J = 7.0 Hz, 3H,

$OCH_2CH_2CH_2(CH_2)_{12}CH_3$). ^{13}C NMR (125.65 MHz, $CDCl_3$, 25 °C): δ (ppm) 168.8, 163.4, 159.0, 156.5, 148.4, 145.2, 145.1, 145.0, 144.7, 144.5, 144.4, 143.7, 142.9, 142.8, 142.1, 142.0, 141.7, 140.8, 140.7, 138.8, 138.7, 132.5, 130.2, 130.0, 121.8, 114.7, 108.6, 107.2, 71.6, 68.3, 67.5, 65.3, 64.9, 52.4, 34.1, 32.0, 29.8, 29.7, 29.4, 29.3, 28.6, 26.1, 25.6, 25.2, 22.8, 14.2.

$Py_2(OH)_2$. A dioxane solution (60 mL) of a mixture of Py_2 (0.57 g, 1.62 mmol), 2-ethyl-2-(hydroxymethyl)-1,3-propanediol (2.11 g, 15.7 mmol), and H_2SO_4 (0.5 mL) was refluxed under Ar in a flask equipped with a Dean-Stark trap. After the complete disappearance of Py_2 was confirmed by TLC, the reaction mixture was poured into water and extracted with CH_2Cl_2. The combined organic extract was dried over Na_2SO_4, concentrated, and chromatographed on silica gel with CH_2Cl_2/MeOH (0–5%, gradient) as an eluent, to allow isolation of $Py_2(OH)_2$ as a white powdery substance (1.35 g) in 37% yield. MS (MALDI-TOF, dithranol, reflector mode): m/z 453.03 ($[M + H]^+$, calcd. for $C_{25}H_{28}N_2O_6$: 452.5). ^1H NMR (500 MHz, $CDCl_3$, 25 °C): δ (ppm) 8.62 (d, J = 5.5 Hz, 4H, *o*-H of CH_2Py), 7.35 (d, J = 5.5 Hz, 4H, *m*-H of CH_2Py), 7.21 (d, J = 1.5 Hz, 2H, *o*-H of $(RO_2C)C_6H_3(OCH_2Py)_2$), 6.77 (t, J = 2.5 Hz, 1H, *p*-H of $(RO_2C)C_6H_3(OCH_2Py)_2$), 5.11 (s, 4H, $(RO_2C)C_6H_3(OCH_2Py)_2$), 4.04 (s, 2H, CCH_2OCOAr), 3.63 (d, J = 6.0 Hz, 4H, $C(CH_2OH)_2$), 1.34 (q, J = 7.5 Hz, 2H, CCH_2CH_3), 0.90 (t, 3H, CCH_2CH_3).

Py_2F_2. To a CH_2Cl_2 solution (10 mL) of a mixture of FCO_2H (372 mg, 0.303 mmol), $Py_2(OH)_2$ (54.9 mg, 0.121 mmol), and DPTS (44.8 mg, 0.152 mmol) was added a CH_2Cl_2 solution (3.1 mL) of DCC (94.4 mg, 0.458 mmol), and the mixture was stirred at room temperature. After 1 day, the reaction mixture was filtrated off from an insoluble fraction, and the filtrate was concentrated and subjected to recycling preparative SEC (2H/3H columns) with THF as an eluent, to allow isolation of Py_2F_2 as a dark brown powdery substance (114 mg) in 33% yield. MS (MALDI-TOF, dithranol, reflector mode): m/z 2867.61 ($[M + 1]^+$, calcd. for $C_{203}H_{112}N_2O_{18}$: 2866.95). ^1H NMR (500 MHz, $CDCl_3$, 25 °C): δ (ppm) 8.60 (d, J = 5.5 Hz, 4H, *o*-H of CH_2Py), 7.35 (d, J = 5.5 Hz, 4H, *m*-H of CH_2Py), 7.18 (d, J = 2.0 Hz, 2H, *o*-H of $(RO_2C)C_6H_3(OCH_2Py)_2$), 7.14 (d, J = 9.0 Hz, 4H, *m*-H of $CH_2C_6H_4O$), 6.76 (d, 3H, *o*-H of $CH_2C_6H_4O$ and *p*-H of $(RO_2C)C_6H_3(OCH_2Py)_2$), 5.09 (s, 4H, $(RO_2C)C_6H_3(OCH_2Py)_2$), 4.63 (t, J = 7.0 Hz, 4H, OCH_2CH_2Ar), 4.56 (s, 4H, $ArOCH_2CO_2R$), 4.43 (t, J = 6.5 Hz, 4H, $OCH_2CH_2(CH_2)_{13}CH_3$), 4.13 (s, 4H, $C(CH_2OCOR)_2$), 4.11 (s, 4H, CCH_2OCOAr), 3.04 (t, J = 7 Hz, 4H, OCH_2CH_2Ar), 1.77 (m,

4H, $OCH_2CH_2CH_2(CH_2)_{12}CH_3$), 1.39 (m, 6H, $OCH_2CH_2CH_2(CH_2)_{12}CH_3$ and CCH_2CH_3), 1.22 (br, 48H, $OCH_2CH_2CH_2(CH_2)_{12}CH_3$), 0.87–0.82 (m, 9H, $OCH_2CH_2CH_2(CH_2)_{12}CH_3$ and CCH_2CH_3). ^{13}C NMR (125.65 MHz, $CDCl_3$, 25 °C): δ (ppm) 168.4, 165.0, 163.4, 159.2, 156.3, 149.6, 145.2, 145.1, 145.0, 144.9, 144.7, 144.5, 144.4, 143.7, 142.9, 142.8, 142.1, 142.0, 141.8, 141.7, 140.8, 140.7, 138.8, 138.7, 130.2, 130.0, 114.6, 108.5, 107.5, 71.5, 68.5, 67.5, 65.0, 64.4, 41.2, 34.1, 33.3, 32.0, 29.8, 29.7, 29.5, 29.3, 28.7, 26.1, 23.4, 22.8, 14.2, 7.5.

3. To a dry DMF solution (250 mL) of a mixture of pentaerythritol (2.06 g, 15.1 mmol) and imidazole (6.22 g, 91.4 mmol) was slowly added *tert*-butylchlorodiphenylsilane (12.84 g, 46.7 mmol) under Ar at 0 ºC, and the mixture was stirred at room temperature overnight. Then, the reaction mixture was poured into saturated aqueous $NaHCO_3$ (500 mL), extracted with AcOEt, and washed with brine. The combined organic extract was dried over Mg_2SO_4, concentrated, and chromatographed on silica gel with CH_2Cl_2 as an eluent, to allow isolation of **3** as a white powdery substance (11.70 g) in 91% yield. MS (MALDI-TOF, dithranol, reflector mode): m/z 873.20 ($[M + Na]^+$, calcd. for $C_{53}H_{66}O_4Si_3$: 851.35). ^{1}H NMR (500 MHz, $CDCl_3$, 25 °C): δ (ppm) 7.54 (d, J = 7.5 Hz, 12H, *o*-H of $Si(C_6H_5)_2{}^tBu$), 7.36 (t, J = 7.5 Hz, 6H, *p*-H of $Si(C_6H_5)_2{}^tBu$), 7.26 (t, J = 7.5 Hz, 12H, *m*-H of $Si(C_6H_5)_2{}^tBu$), 3.78 (d, J = 6.0 Hz, 2H, $C(CH_2OTBDPS)_3(CH_2OH)$), 3.72 (s, 6H, $C(CH_2OTBDPS)_3(CH_2OH)$), 2.75 (t, J = 6.0 Hz, 6H, $C(CH_2OTBDPS)_3(CH_2OH)$), 0.93 (s, 27H, $Si(Ph)_2C(CH_3)_3$).

4. To a dry DMF solution (70 mL) of a mixture of 3,5-dihydroxybenzoic acid (5.04 g, 32.7 mmol) and imidazole (8.02 g, 117.8 mmol) was slowly added a DMF solution (30 mL) of *tert*-butylchlorodimethylsilane (17.9 g, 118.7 mmol) under Ar at 0 ºC, and the mixture was stirred at room temperature overnight. Then, the reaction mixture was poured into saturated aqueous $NaHCO_3$ (500 mL), extracted with ether, and washed with brine. The combined organic extract was dried over $MgSO_4$, concentrated, and chromatographed on silica gel with CH_2Cl_2/hexane (v/v: 1/1) as an eluent, to allow isolation of **4** as a white powdery substance (13.56 g) in 83 % yield. MS (MALDI-TOF, dithranol, reflector mode): m/z 497.19 ($[M + H]^+$, calcd. for $C_{25}H_{48}O_4Si_3$: 496.9). ^{1}H NMR (500 MHz, $CDCl_3$, 25 °C): δ (ppm) 7.11 (d, J = 2.5 Hz, 2H, *o*-H of $C_6H_3CO_2TBDMS$), 6.51 (t, J = 2.5 Hz, 1H, *p*-H of $C_6H_3CO_2TBDMS$), 0.99 (s, 9H, $ArCO_2Si(Me)_2C(CH_3)_3$), 0.96 (s, 18H, $ArOSi(Me)_2C(CH_3)_3$), 0.34 (s, 6H, $ArCO_2Si(CH_3)_2{}^tBu$), 0.19 (s, 12H, $ArOSi(CH_3)_2{}^tBu$).

5. To a THF/MeOH solution (40/120 mL) of **4** (7.20 g, 14.5 mmol) was added aqueous K_2CO_3 (0.72 M, 40 mL), and the mixture was stirred at room temperature. After 1 h, the reaction mixture was concentrated to a 1/4 volume and diluted with brine (200 mL). After the pH was adjusted at 4–5 with $KHSO_4$ (1.0 M), the resulting mixture was extracted with ether and wash with brine. The combined organic extract was dried over Na_2SO_4, concentrated, and chromatographed on silica gel with CH_2Cl_2/THF (0–5%, gradient) as an eluent, to allow isolation of **5** as a white powdery substance (2.14 g) in 38 % yield. MS (MALDI-TOF, reflector mode without matrix): m/z 382.10 ($[M + H]^+$, calcd. for $C_{19}H_{34}O_4Si_2$: 382.64). ^{1}H NMR (500 MHz, $CDCl_3$, 25 °C): δ (ppm) 7.17 (d, J = 2.0 Hz, 2H, *o*-H of $C_6H_3CO_2H$), 6.55 (t, J = 2.0 Hz, 1H, *p*-H of $C_6H_3CO_2H$), 0.97 (s, 18H, $ArOSi(Me)_2C(CH_3)_3$), 0.20 (s, 12H, $ArOSi(CH_3)_2{}^tBu$).

6. To a CH_2Cl_2 solution (10 mL) of a mixture of **3** (2.62 mg, 3.08 mmol), **5** (1.11 mg, 2.90 mmol), and DPTS (175 mg, 0.595 mmol) was added a CH_2Cl_2 solution (10 mL) of DCC (969 mg, 4.70 mmol), and the mixture was stirred at room temperature. After 2 days, the reaction mixture was filtrated off from an insoluble fraction, and the filtrate was concentrated. The residue was chromatographed on silica gel with CH_2Cl_2/hexane (v/v: 1/1) as an eluent, to allow isolation of **6** as a white powdery substance (3.14 g) in 89% yield. MS (MALDI-TOF, CHCA as matrix, reflector mode): m/z 1237.51 ($[M + Na]^+$, calcd. for $C_{72}H_{98}O_7Si_5$: 1215.97). ^{1}H NMR (500 MHz, $CDCl_3$, 25 °C): δ (ppm) 7.55 (d, J = 8.0 Hz, 12H, *o*-H of $Si(C_6H_5)_2{}^tBu$), 7.32 (t, J = 8.0 Hz, 6H, *p*-H of $Si(C_6H_5)_2{}^tBu$), 7.22 (t, J = 7.5 Hz, 12H, *m*-H of $Si(C_6H_5)_2{}^tBu$), 6.97 (m, 2H, *o*-H of $C_6H_3CO_2R$), 6.54 (m, 1H, *p*-H of $C_6H_3CO_2R$), 4.46 (s, 2H, $C(CH_2OTBDPS)_3(CH_2OCOAr)$), 3.86 (s, 6H, $C(CH_2OTBDPS)_3(CH_2OCOAr)$), 0.97 (s, 18H, $ArOSi(Me)_2C(CH_3)_3$), 0.95 (s, 27H, $Si(Ph)_2C(CH_3)_3$), 0.14 (s, 12H, $ArOSi(CH_3)_2{}^tBu$).

7. To a THF solution (40 mL) of **6** (3.14 g, 2.58 mmol) was added a THF solution of tetrabutylammonium fluoride (TBAF, 1.0 M, 5.1 mL), and the mixture was stirred at room temperature. After 5 h, the reaction mixture was poured into saturated aqueous NH_4Cl (300 mL), extracted with ether, and wash with brine. The combined organic extract was dried over Na_2SO_4, concentrated, and chromatographed on silica gel with CH_2Cl_2/MeOH (0–3%, gradient) as an eluent, to allow isolation **7** as a white powdery substance (2.34 g) in 92 % yield. MS (MALDI-TOF, CHCA as matrix, reflector mode): m/z 1009.41 ($[M + Na]^+$, calcd. for

$C_{60}H_{70}O_7Si_3$: 987.45). ^{1}H NMR (500 MHz, $CDCl_3$, 25 °C): δ (ppm) 7.57 (d, J = 6.5 Hz, 12H, *o*-H of $Si(C_6H_5)_2{}^tBu$), 7.35 (t, J = 7.0 Hz, 6H, *p*-H of $Si(C_6H_5)_2{}^tBu$), 7.25 (t, J = 7.0 Hz, 12H, *m*-H of $Si(C_6H_5)_2{}^tBu$), 6.98 (d, J = 2.5 Hz, 2H, *o*-H of $(HO)_2C_6H_3CO_2R$), 6.57 (t, J = 2.5 Hz, 1H, *p*-H of $(HO)_2C_6H_3CO_2R$), 4.44 (s, 2H, $C(CH_2OTBDPS)_3(CH_2OCOAr)$), 3.86 (s, 6H, $C(CH_2OTBDPS)_3(CH_2OCOAr)$), 0.97 (s, 27H, $Si(Ph)_2C(CH_3)_3$).

8. To a THF solution (10 mL) of a mixture of **7** (1.22 g, 1.24 mmol), 4-hydoxymethylpyridine (0.341 g, 3.12 mmol), and PPh_3 (0.813 g, 3.10 mmol) was slowly added DEAD (0.553 g, 3.18 mmol) under Ar, and the mixture was stirred at room temperature. After 7 days, the reaction mixture was concentrated and subjected to recycling preparative SEC (1H/2H) using $CHCl_3$ as an eluent, where the first fraction was collected and evaporated to dryness, and the residue was subjected to preparative TLC (SiO_2) with $CHCl_3$/MeOH (5%) as an eluent, affording **8** as white powdery substance (0.98 g) in 68% yield. MS (MALDI-TOF, dithranol as matrix, reflector mode): m/z 1169.36 ($[M + H]^+$, calcd. for $C_{72}H_{80}N_2O_7Si_3$: 1169.67). ^{1}H NMR (500 MHz, $CDCl_3$, 25 °C): δ (ppm) 8.60 (d, J = 4.5 Hz, 4H, *o*-H of Py), 7.53 (d, J = 8.0 Hz, 12H, *o*-H of $Si(C_6H_5)_2{}^tBu$), 7.30–7.25 (m, 10H, *p*-H of $Si(C_6H_5)_2{}^tBu$ and *m*-H of Py), 7.18 (t, J = 8.0 Hz, 12H, *m*-H of $Si(C_6H_5)_2{}^tBu$), 7.00 (d, J = 2.5 Hz, 2H, *o*-H of $(PyCH_2O)_2C_6H_3CO_2R$), 6.75 (t, J = 2.5 Hz, 1H, *p*-H of $(PyCH_2O)_2C_6H_3CO_2R$), 4.94 (s, 4H, OCH_2Py), 4.54 (s, 2H, $C(CH_2OTBDPS)_3(CH_2OCOAr)$), 3.833 (s, 6H, $C(CH_2OTBDPS)_3(CH_2OCOAr)$), 0.93 (s, 27H, $Si(Ph)_2C(CH_3)_3$).

$Py_2(OH)_3$. To a THF solution (10 mL) of **8** (0.46 g, 0.393 mmol) was added Et_4NF (TBAF) (0.584 g, 2.23 mmol), and the mixture was stirred at room temperature. After 1 day, the reaction mixture was evaporated to dryness, and the residue was subjected to recycling preparative SEC (1H/2H) with THF as an eluent, where the first fraction was collected and subjected to preparative TLC (SiO_2) with CH_2Cl_2/MeOH (10%) as an eluent, affording $Py_2(OH)_3$ as a white powdery substance (66 mg) in 37% yield. MS (MALDI-TOF, dithranol as matrix, reflector mode): m/z 456.20 ($[M + H]^+$, calcd. for $C_{24}H_{26}N_2O_7$: 454.47). ^{1}H NMR (500 MHz, CD_3OD, 25 °C): δ (ppm) 8.20 (d, J = 5.0 Hz, 4H, *o*-H of Py), 7.50 (t, J = 5.0 Hz, 4H, *m*-H of Py), 7.25 (d, J = 2.5 Hz, 2H, *o*-H of $(PyCH_2O)_2C_6H_3CO_2R$), 6.93 (t, J = 2.5 Hz, 1H, *p*-H of $(PyCH_2O)_2C_6H_3CO_2R$), 5.22 (s, 4H, OCH_2Py), 4.30 (s, 2H, $C(CH_2OH)_3(CH_2OCOAr)$), 3.63 (s, 6H, $C(CH_2OH)_3(CH_2OCOAr)$).

Py_2F_3. To a CH_2Cl_2/THF solution (5/5 mL) of a mixture of FCO_2H (498 mg, 0.406 mmol), $Py_2(OH)_3$ (48.3 mg, 0.106 mmol), and DPTS (92 mg, 0.313 mmol) was added a CH_2Cl_2 solution (5 mL) of DCC (141 mg, 0.681 mmol) under Ar, and the mixture was stirred at room temperature. After 2 days, the reaction mixture was filtrated off from an insoluble fraction, and the filtrate was evaporated to dryness. Then, the residue was subjected to recycling preparative SEC (2H/3H columns) with $CHCl_3$ as an eluent, to allow isolation of Py_2F_3 as a dark brown powdery substance (183 mg) in 42% yield. MS (MALDI-TOF, dithranol, reflector mode): m/z 4077.81 ($[M + 1]^+$, calcd. for $C_{291}H_{152}N_2O_{25}$: 4076.19). ^{1}H NMR (500 MHz, $CDCl_3$, 25 °C): δ (ppm) 8.63 (br, 4H, *o*-H of CH_2Py), 7.53 (br, 4H, *m*-H of CH_2Py), 7.18 (br, 2H, *o*-H of $(RO_2C)C_6H_3(OCH_2Py)_2$), 7.15 (d, J = 8.0 Hz, 6H, *m*-H of $CH_2C_6H_4O$), 6.82 (br, 1H, *p*-H of $(RO_2C)C_6H_3(OCH_2Py)_2$), 6.75 (d, J = 8.5 Hz, 6H, *o*-H of $CH_2C_6H_4O$), 5.15 (s, 4H, $(RO_2C)C_6H_3(OCH_2Py)_2$), 4.63 (t, J = 6.5 Hz, 6H, OCH_2CH_2Ar), 4.56 (s, 6H, $ArOCH_2CO_2R$), 4.43 (t, J = 6.5 Hz, 6H, $OCH_2CH_2(CH_2)_{13}CH_3$), 4.15 (s, 6H, $C(CH_2OCOR)_3$), 4.14 (s, 2H, CCH_2OCOAr), 3.04 (t, J = 6.5 Hz, 6H, OCH_2CH_2Ar), 1.78 (m, 6H, $OCH_2CH_2CH_2(CH_2)_{12}CH_3$), 1.42 (m, 6H, $OCH_2CH_2CH_2(CH_2)_{12}CH_3$), 1.32–1.22 (br, 72H, $OCH_2CH_2CH_2(CH_2)_{12}CH_3$), 0.85 (t, J = 6.5 Hz, 9H, $OCH_2CH_2CH_2(CH_2)_{12}CH_3$). ^{13}C NMR (125.65 MHz, $CDCl_3$, 25 °C): δ (ppm) 168.2, 163.4, 159.0, 156.2, 145.2, 145.1, 145.0, 144.9, 144.7, 144.6, 144.5, 144.4, 143.7, 143.0, 142.9, 142.8, 142.1, 142.0, 141.8, 141.7, 140.8, 140.7, 138.9, 138.7, 130.4, 130.1, 114.6, 108.7, 71.6, 68.3, 67.6, 67.5, 64.7, 62.5, 52.4, 42.7, 34.1, 32.1, 29.8, 29.7, 29.5, 29.3, 28.7, 26.1, 22.8, 14.3.

3. Mass Spectrometry of Py_2F_n (n = 1–3)

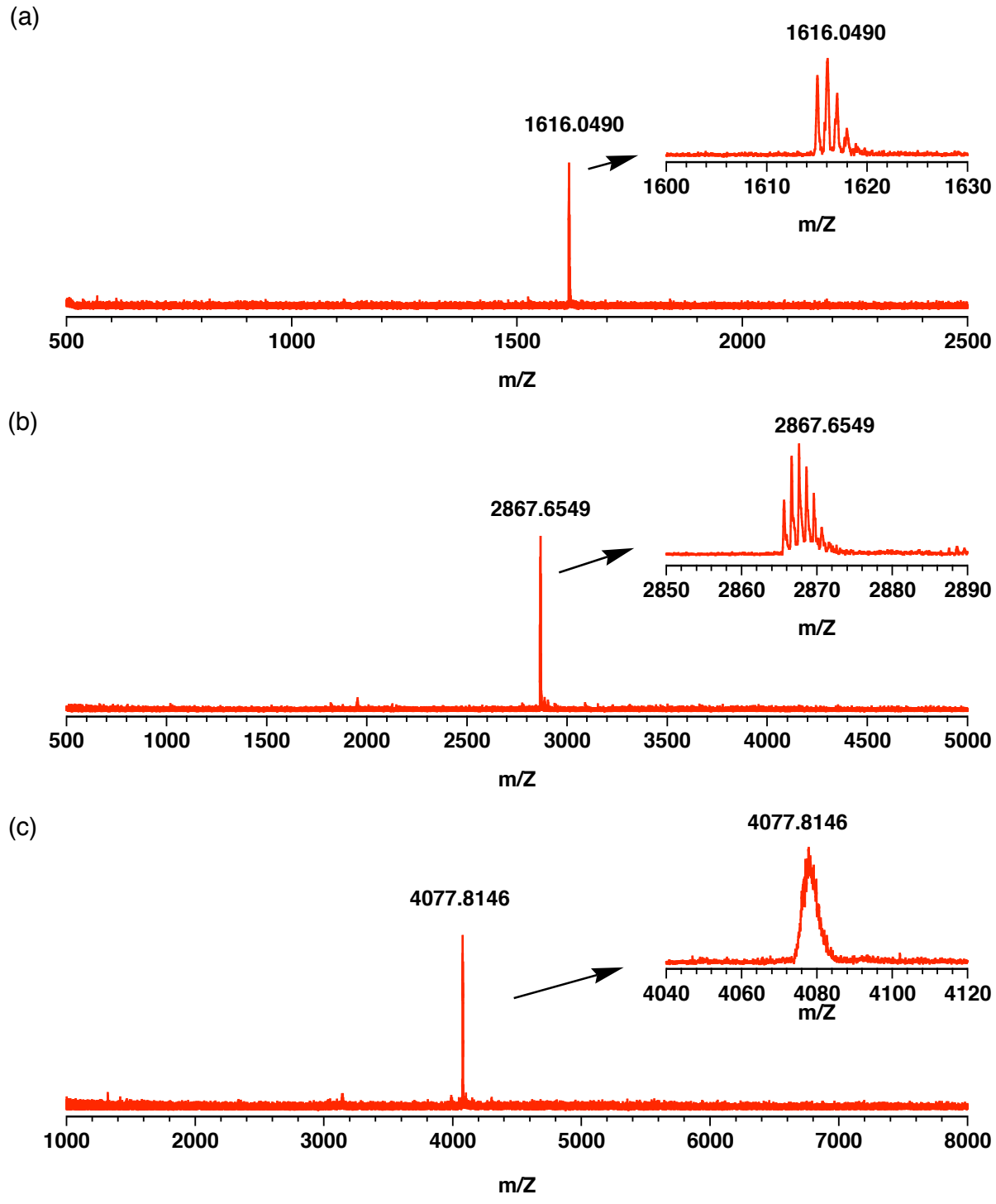

Figure *S1.* MALDI-TOF-MS spectra of (a) Py_2F_1, (b) Py_2F_2, and (c) Py_2F_3 using dithranol as a matrix in a reflector mode.

4. Absorption Spectroscopy of Py_2F_n (n = 1–3)

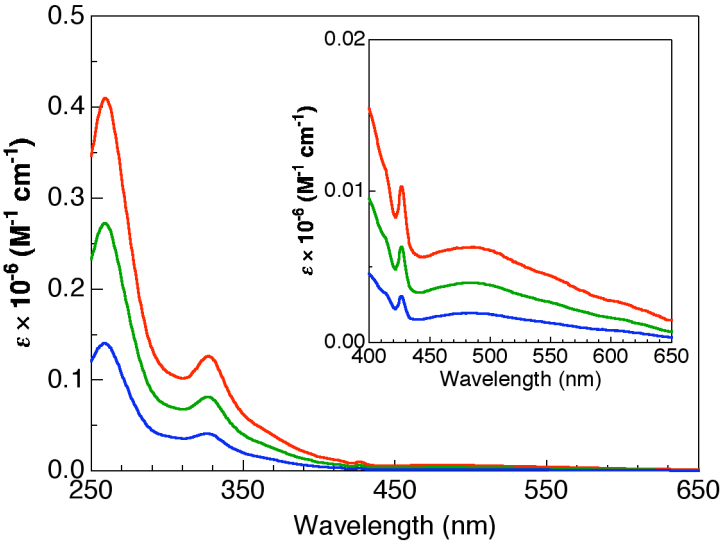

Figure *S2.* Electronic absorption spectra of Py_2F_1 (blue), Py_2F_2 (green), and Py_2F_3 (red) in $CHCl_3$ at 25 ºC. Inset: spectra at 400–650 nm.

5. Definition and Evaluation of Average Binding Affinities (*K*) of the Zinc Porphyrin Units in DP_m (*m* = 6, 12, and 24) toward the Pyridine Units in Py_2F_n (*n* = 1–3)

Typically, a $CHCl_3$ solution (3 mL) of DP_{24} (1.5×10^{-7} M) was titrated by stepwise addition of a $CHCl_3$ solution of Py_2F_3 (5.1×10^{-4} M) and subjected to absorption spectroscopy at 25 ºC. All the spectra were corrected with a dilution factor and background subtraction. By simply assuming a one-to-one coordination between the zinc porphyrin and pyridine units in DP_{24} and Py_2F_3, respectively, the average binding affinities (*K*) were evaluated, from the spectral change upon titration (Figures 1a and 1b), by non–linear curve fitting using the following equation: $\Delta A = \Delta A_\infty((1 + K[\mathrm{Py}] + K[\mathrm{P_{Zn}}]_0) - ((1 + K[\mathrm{Py}] + K[\mathrm{P_{Zn}}]_0)^2 - 4\,K^2[\mathrm{P_{Zn}}]_0[\mathrm{Py}])^{0.5})/(2\,K[\mathrm{P_{Zn}}]_0)$, where $[\mathrm{Py}] = 2 \times [\mathrm{Py_2F_3}]$, $[\mathrm{P_{Zn}}] = 24 \times [\mathrm{DP_{24}}]$, $\Delta A = A - A_0$, and $\Delta A_\infty = A_\infty - A_0$. Here, A_0 denotes the absorbance in the absence of Py_2F_3, while A and A_∞ represent those in the presence of Py_2F_3 at given and infinite concentrations of Py, respectively.[3]

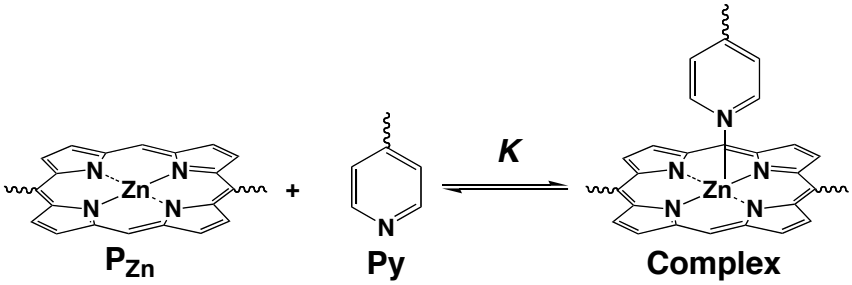

$$K = \frac{[\mathrm{Complex}]}{[\mathrm{P_{Zn}}][\mathrm{Py}]}$$

[3] Connors, K.A. *Binding Constants*, Wiley, New York, **1987**.

6. Spectroscopic Titration of DP_m (m = 6, 12, and 24) and P_1 with Py_2F_n (n = 1–3)

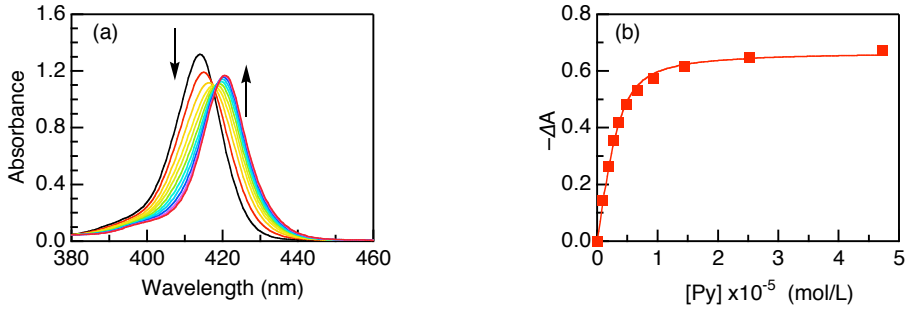

Figure S3. (a) Electronic absorption spectral change of DP_6 (6.0×10^{-7} M) upon titration with Py_2F_1 ($[Py_2F_1]/[DP_6]$ = 0, 0.74, 1.5, 2.2, 2.9, 4.0, 5.5, 7.7, 12, 21, and 39) in $CHCl_3$ at 25 ºC. (b) Change in absorbance at 414.0 and its curve–fitting profile (solid curve).

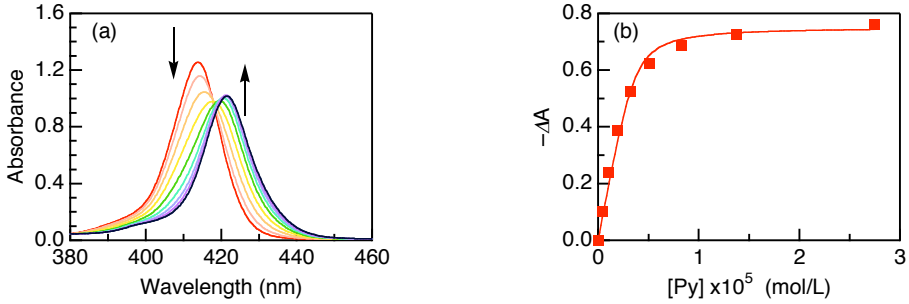

Figure S4. (a) Electronic absorption spectral change of DP_6 (6.0×10^{-7} M) upon titration with Py_2F_2 ($[Py_2F_2]/[DP_6]$ = 0, 0.35, 0.88, 1.6, 2.7, 4.2, 6.9, 12, and 23) in $CHCl_3$ at 25 ºC. (b) Change in absorbance at 413.8 nm and its curve–fitting profile (solid curve).

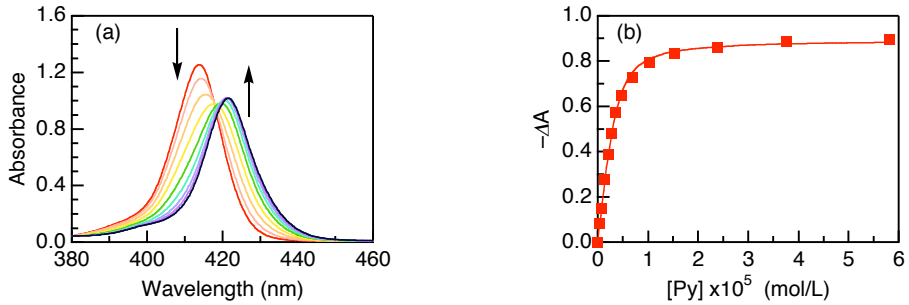

Figure S5. (a) Electronic absorption spectral change of DP_6 (6.0×10^{-7} M) upon titration with Py_2F_3 ($[Py_2F_3]/[DP_6]$ = 0, 0.35, 0.88, 1.6, 2.7, 4.2, 6.9, 12, and 23) in $CHCl_3$ at 25 ºC. (b) Change in absorbance at 413.8 and its curve–fitting profile (solid curve).

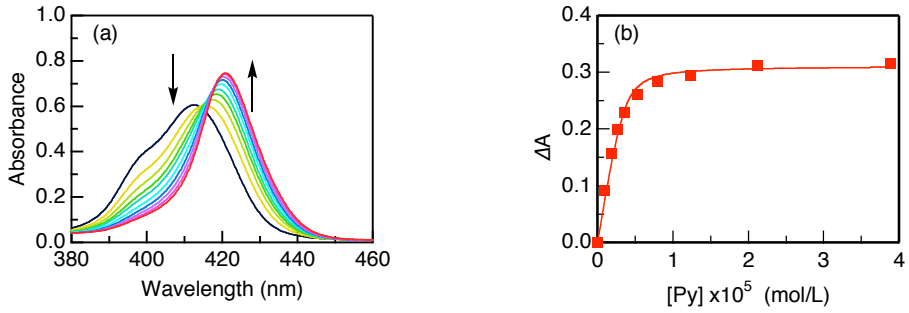

Figure S6. (a) Electronic absorption spectral change of DP_{12} (3.0×10^{-7} M) upon titration with Py_2F_1 ($[Py_2F_1]/[DP_{12}]$ = 0, 1.5, 2.9, 4.4, 5.9, 8.8, 13, 21, 35, and 65) in $CHCl_3$ at 25 ºC. (b) Change in absorbance at 420.8 nm and its curve–fitting profile (solid curve).

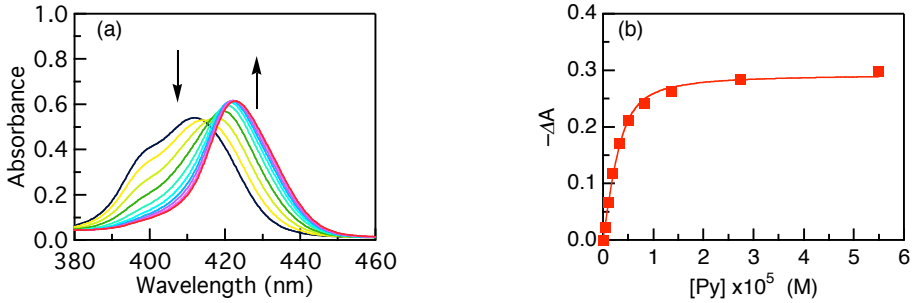

Figure S7. (a) Electronic absorption spectral change of DP_{12} (3.0×10^{-7} M) upon titration with Py_2F_2 ($[Py_2F_2]/[DP_{12}]$ = 0, 0.71, 1.8, 3.2, 5.3, 8.5, 14, 23, 46, and 92) in $CHCl_3$ at 25 ºC. (b) Change in absorbance at 411.8 nm and its curve–fitting profile (solid curve).

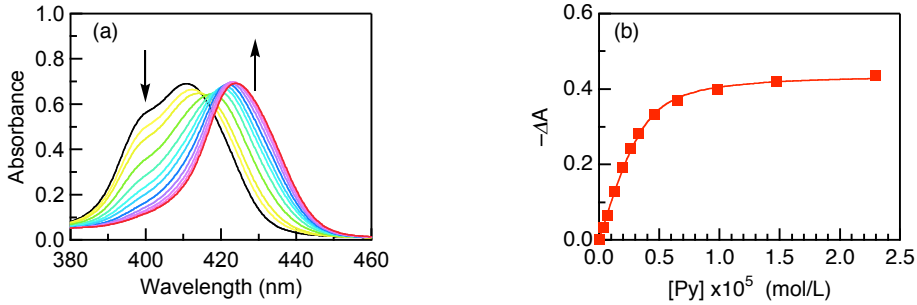

Figure S8. (a) Electronic absorption spectral change of DP_{12} (3.0×10^{-7} M) upon titration with Py_2F_3 ($[Py_2F_3]/[DP_{12}]$ = 0, 0.55, 1.1, 2.2, 3.3, 4.4, 5.5, 7.7, 11, 16, 25, and 38) in $CHCl_3$ at 25 ºC. (b) Change in absorbance at 410.8 nm and its curve–fitting profile (solid curve).

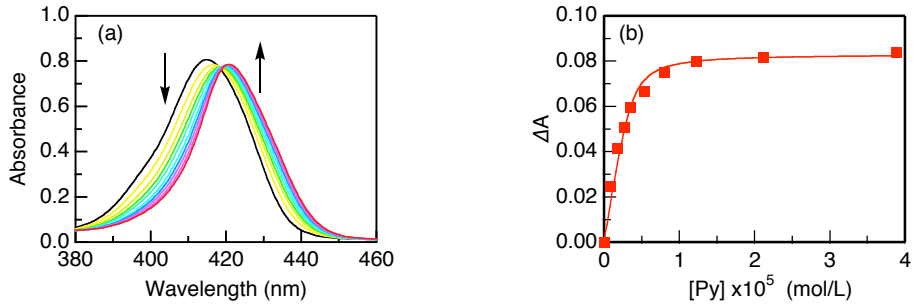

Figure S9. (a) Electronic absorption spectral change of DP_{24} (1.5×10^{-7} M) upon titration with Py_2F_1 ([Py_2F_1]/[DP_{24}] = 0, 3.0, 5. 9, 8.8, 12, 18, 27, 41, 71, and 130) in $CHCl_3$ at 25 ºC. (b) Change in absorbance at 421.0 nm and its curve–fitting profile (solid curve).

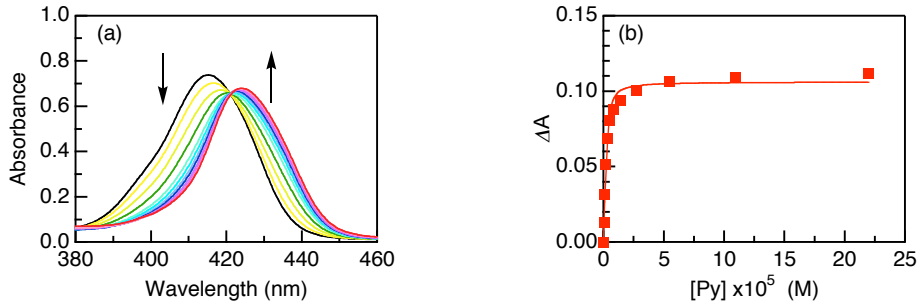

Figure S10. (a) Electronic absorption spectral change of DP_{24} (1.5×10^{-7} M) upon titration with Py_2F_2 ([Py_2F_2]/[DP_{24}] = 0, 1.4, 3.5, 6.4, 11, 17, 28, 46, 92, 183, 366, and 732) in $CHCl_3$ at 25 ºC. (b) Change in absorbance at 415.0 nm and its curve–fitting profile (solid curve).

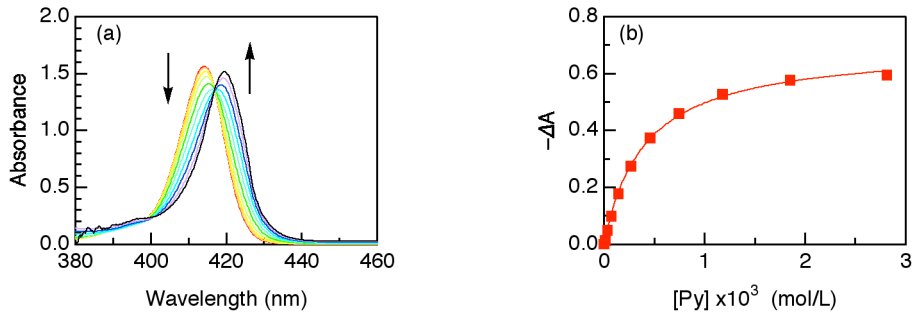

Figure S11. (a) Electronic absorption spectral change of P_1 (3.6×10^{-6} M) upon titration with Py_2F_1 ([Py_2F_1]/[P_1] = 0, 1.3, 4.7, 10, 20, 37, 63, 103, 164, and 257) in $CHCl_3$ at 25 ºC. (b) Change in absorbance at 414.2 nm and its curve–fitting profile (solid curve).

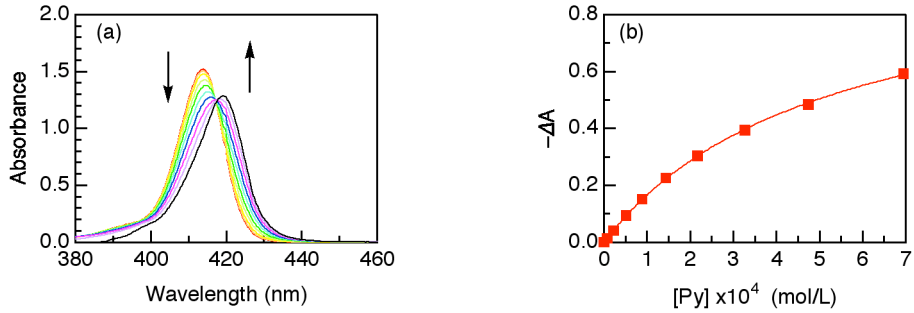

Figure S12. (a) Electronic absorption spectral change of P_1 (3.6×10^{-6} M) upon titration with Py_2F_2 ($[Py_2F_2]/[P_1] = 0$, 1.0, 3.1, 7.1, 12, 20, 30, 45, 66, and 96) in $CHCl_3$ at 25 °C. (b) Change in absorbance at 413.8 nm and its curve–fitting profile (solid curve).

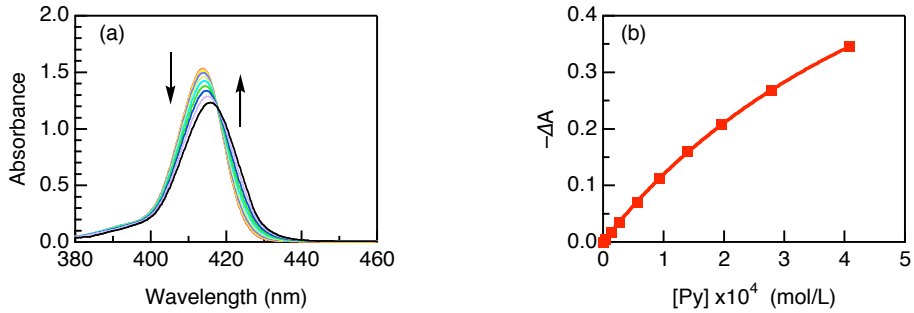

Figure S13. (a) Electronic absorption spectral change of P_1 (3.6×10^{-6} M) upon titration with Py_2F_3 ($[Py_2F_3]/[P_1] = 0$, 0.65, 2.0, 3.9, 7.7, 13, 19, 27, 39, and 57) in $CHCl_3$ at 25 °C. (b) Change in absorbance at 413.8 nm and its curve–fitting profile (solid curve).

7. Gel Permeation Chromatography (GPC) and Composition Analysis of $DP_m \supset Py_2F_n$ (m = 6, 12, and 24; n = 1–3)

Typically, a $CHCl_3$ solution of a mixture of DP_{24} and 25 equivalents of Py_2F_3 was subjected to GPC (Biobeads, S-X1, Bio-rad) with $CHCl_3$ as an eluent, where absorbances at 423 (zinc porphyrin) and 326 (fullerene and zinc porphyrin) nm of each fraction were measured to obtain chromatograms (*e.g.*, Figure S14a). Fractions containing $DP_m \supset Py_2F_n$ were combined and subjected to absorption spectroscopy (Figure S14b). The compositions of $DP_m \supset Py_2F_n$ were determined by integration of the chromatograms, by reference to the calibration curve prepared with varying mole ratios of DP_m and Py_2F_n (inset in Figure S14b).

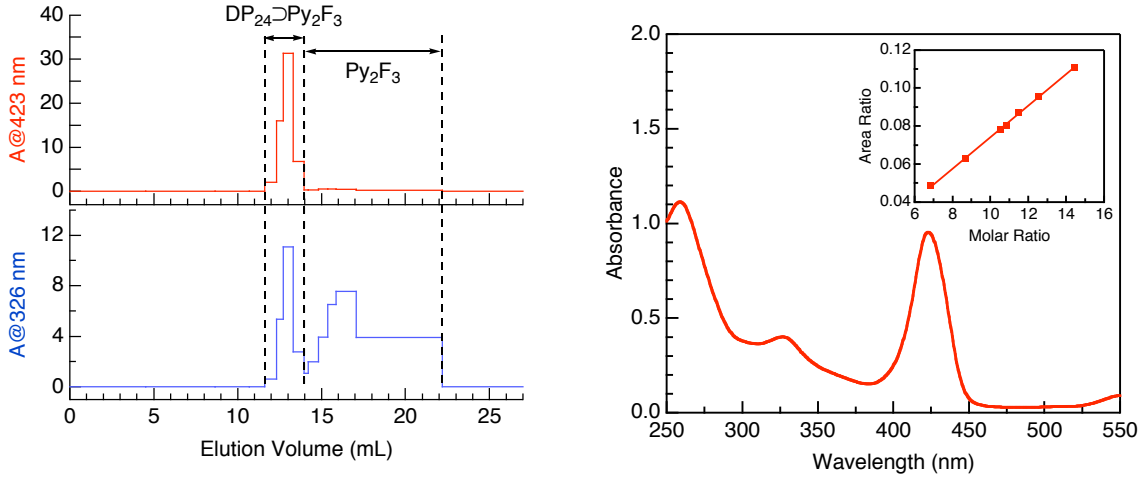

Figure S14. (a) GPC chromatograms (eluent: $CHCl_3$) of a mixture of DP_{24} and 25 equivalents of Py_2F_3 monitored at 423 (red) and 326 (blue) nm. (b) Absorption spectrum of $DP_{24} \supset Py_2F_3$ isolated by GPC at an elution volume from 11.6 to 14.0 mL. Inset: calibration curve (absorbance at 423 nm relative to that of 326 nm versus molar ratio of Py_2F_3 to DP_{24}) for composition determination.

8. Fluorescence Titration of DP_m (m = 6, 12, and 24) with Py_2F_n (n = 1–3)

Sample solutions were bubbled with Ar for at least 30 min prior to measurements. Typically, a $CHCl_3$ solution (3 mL) of DP_{24} (1.5×10^{-7} M) was titrated by stepwise addition of a $CHCl_3$ solution of Py_2F_3 (7.7×10^{-7} M) under Ar and subjected to fluorescence spectroscopy upon excitation at 550.0 nm (isosbestic point or quasi-isosbestic point in the electronic absorption spectral change) at 25 ºC. Stern-Volmer constants (K_{SV}) were evaluated using the equation: $I_0/I = 1 + K_{SV}[Py_2F_3]$, where I_0 and I are the fluorescence intensities in the absence and presence of Py_2F_3.

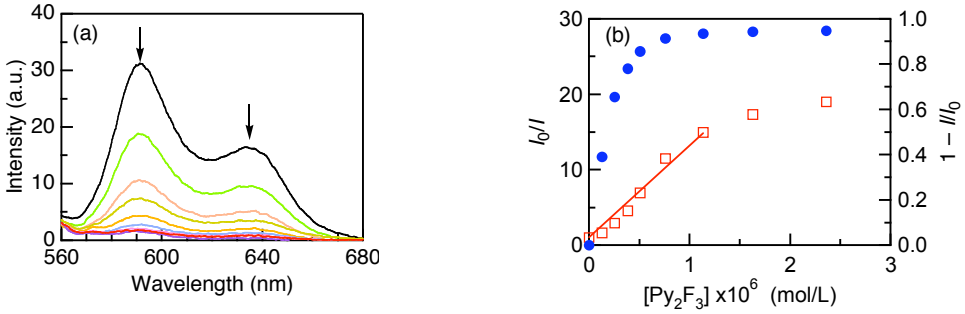

Figure S15. (a) Fluorescence spectral change of DP_{24} (1.5×10^{-7} M, λ_{ext} = 550 nm) upon titration with Py_2F_3 ($[Py_2F_3]/[DP_{24}]$ = 0, 0.9, 1.7, 2.6, 3.4, 5.1, 7.7, 11.1, and 16.2) in $CHCl_3$ at 25 ºC under Ar. (b) Stern-Volmer plot (red open squares and solid line) and degree of fluorescence quenching ($1 - I/I_0$, blue solid circles) monitored at 590 nm in Figure S15a.

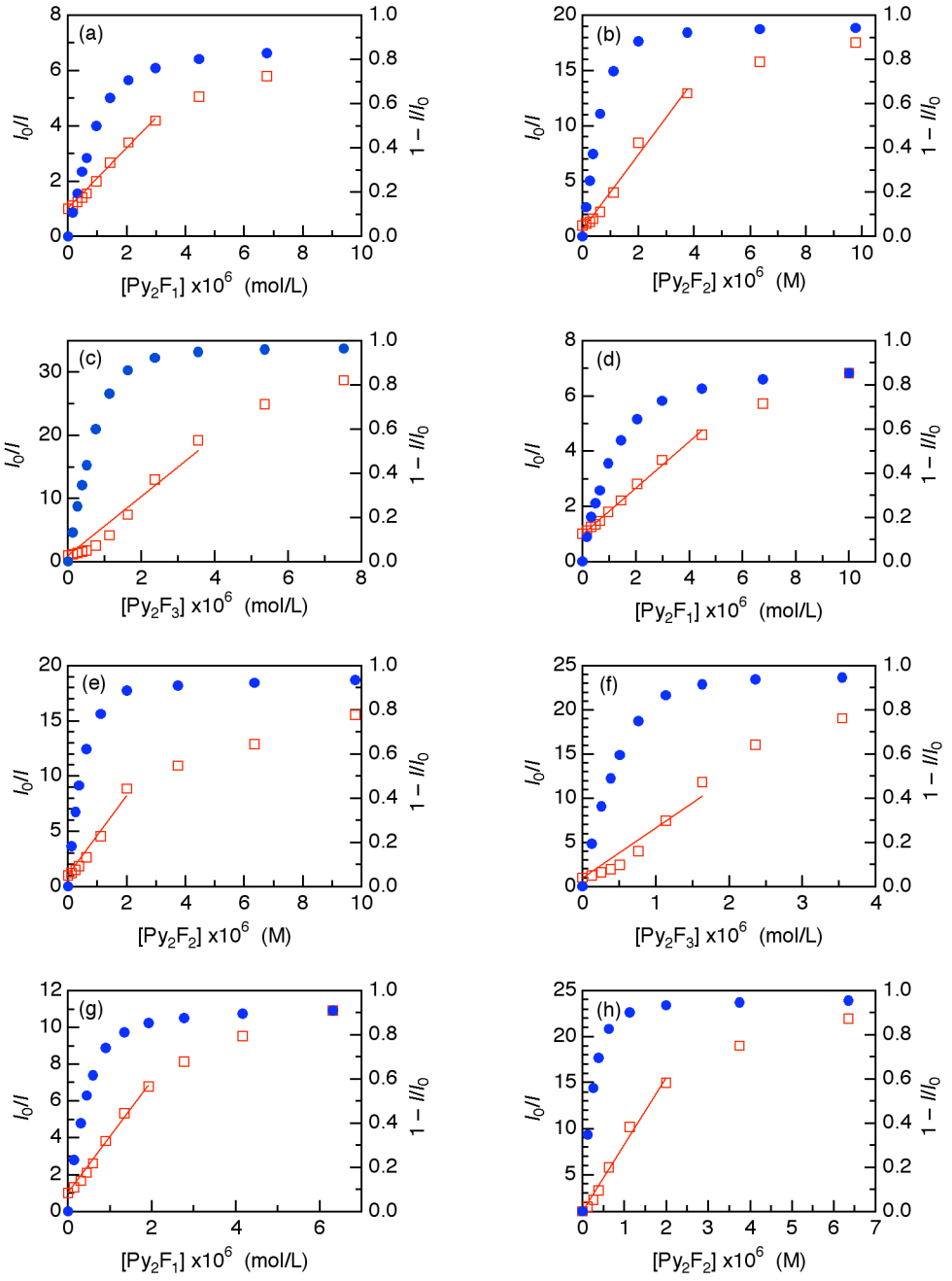

Figure S16. Stern-Volmer plots (red open squares and solid lines) and degrees of fluorescence quenching ($1 - I/I_0$, blue solid circles) upon fluorescence titration of (a) DP_6 (6.0×10^{-7} M) with Py_2F_1, (b) DP_6 (6.0×10^{-7} M) with Py_2F_2, (c) DP_6 (6.0×10^{-7} M) with Py_2F_3, (d) DP_{12} (3.0×10^{-7} M) with Py_2F_1, (e) DP_{12} (3.0×10^{-7} M) with Py_2F_2, (f) DP_{12} (3.0×10^{-7} M) with Py_2F_3, (g) DP_{24} (1.5×10^{-7} M) with Py_2F_1, and (h) DP_{24} (1.5×10^{-7} M) with Py_2F_2, monitored at 590 nm upon excitation at a Q-band in $CHCl_3$ at 25 ºC under Ar.

9. Steady-State Fluorescence Spectroscopy of $DP_6 \supset Py_2F_3$ and Py_2F_3 Alone

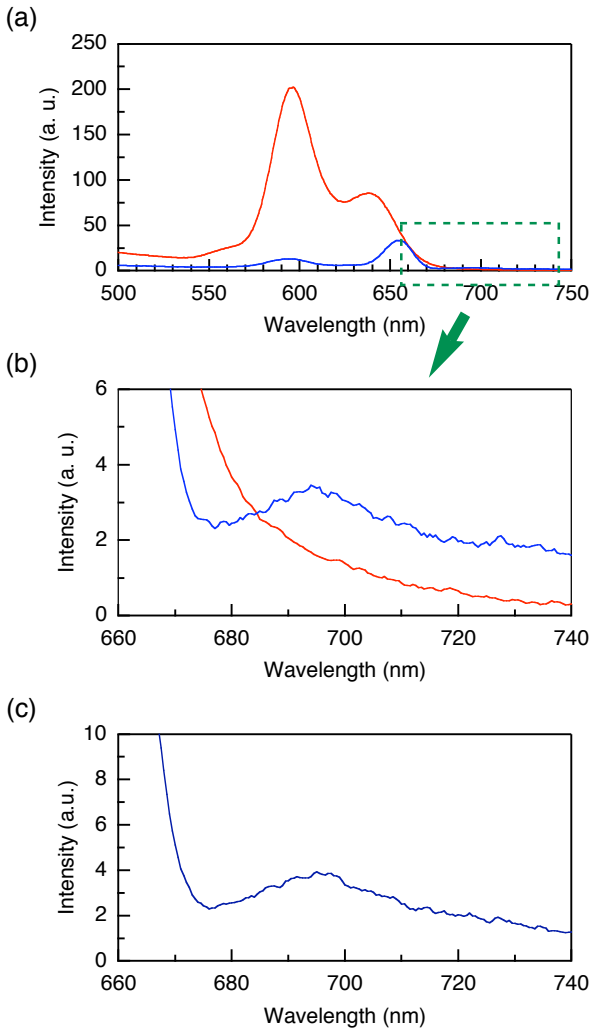

Figure S17. (a) Steady-state fluorescence spectra of DP_6 (1.07×10^{-6} M) in the presence of Py_2F_3 (1.37×10^{-5} M) upon excitation at 327 (fullerene in Py_2F_3 predominantly; blue) and 423 nm (zinc porphyrin predominantly; red) in CH_2Cl_2 at 25 ºC. (b) Enlarged spectra at 660–740 nm of Figure S17a. (c) Steady-state fluorescence spectrum of Py_2F_3 alone (1.37×10^{-5} M) upon excitation at 327 nm in CH_2Cl_2 at 25 ºC.

By reference to Figure S17c, Figure S17a (blue) clearly shows that $DP_6 \supset Py_2F_3$, upon predominant excitation of the fullerene units in Py_2F_3, emits the fullerene fluorescence. However, no fluorescence emission from the fullerene units of Py_2F_3 results, upon predominant excitation of the zinc porphyrin units of DP_6 in $DP_6 \supset Py_2F_3$ (red). These contrasting results clearly exclude a possibility of the zinc porphyrin-to-fullerene energy transfer in $DP_6 \supset Py_2F_3$.

10. Fluorescence Decay Profiles of DP_m (m = 6, 12, and 24) and P_1 in the Presence of Py_2 and Py_2F_n (n = 1–3)

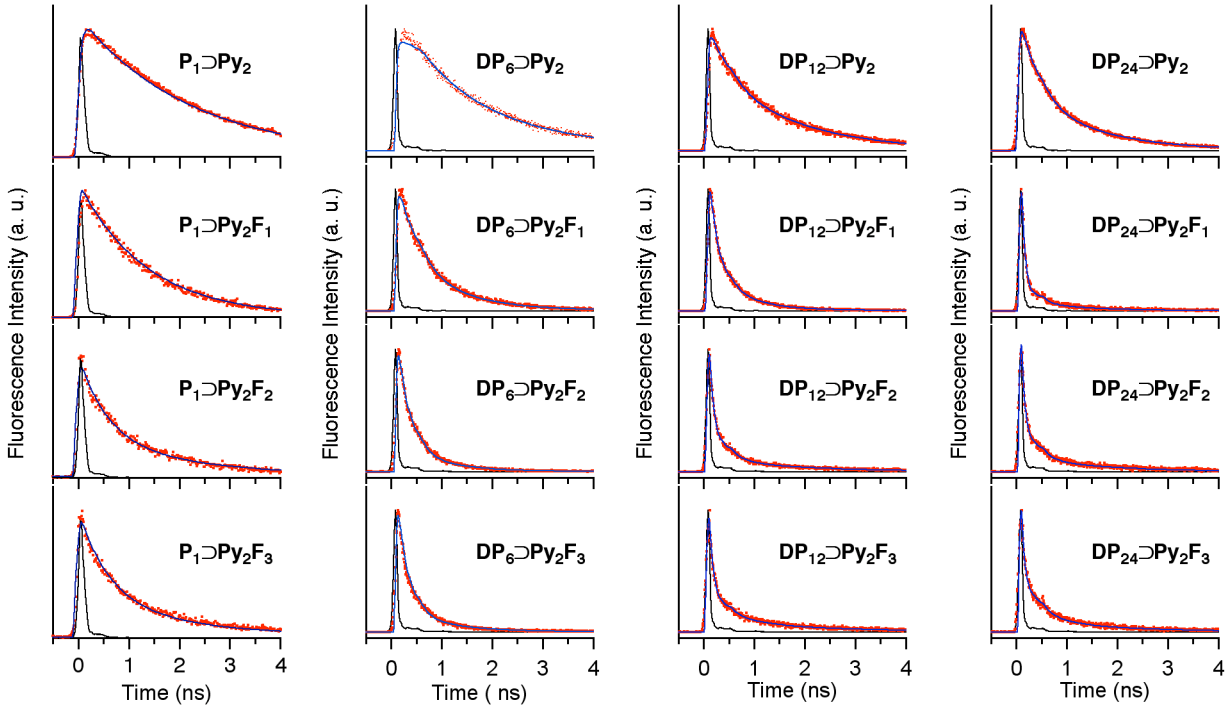

Figure S18. Fluorescence decay profiles at 590 nm of P_1, DP_6, DP_{12}, and DP_{24} in the presence of Py_2, Py_2F_1, Py_2F_2, and Py_2F_3 ([zinc porphyrin] = 3.6×10^{-6} M, [pyridine]/[zinc porphyrin] = 400 for P_1 and 1 for DP_m) upon excitation at 420 nm in CH_2Cl_2 at 20 ºC.

11. Transient Absorption Spectroscopy of $DP_m \supset Py_2F_n$ (m = 6, 12, and 24; n = 1–3)

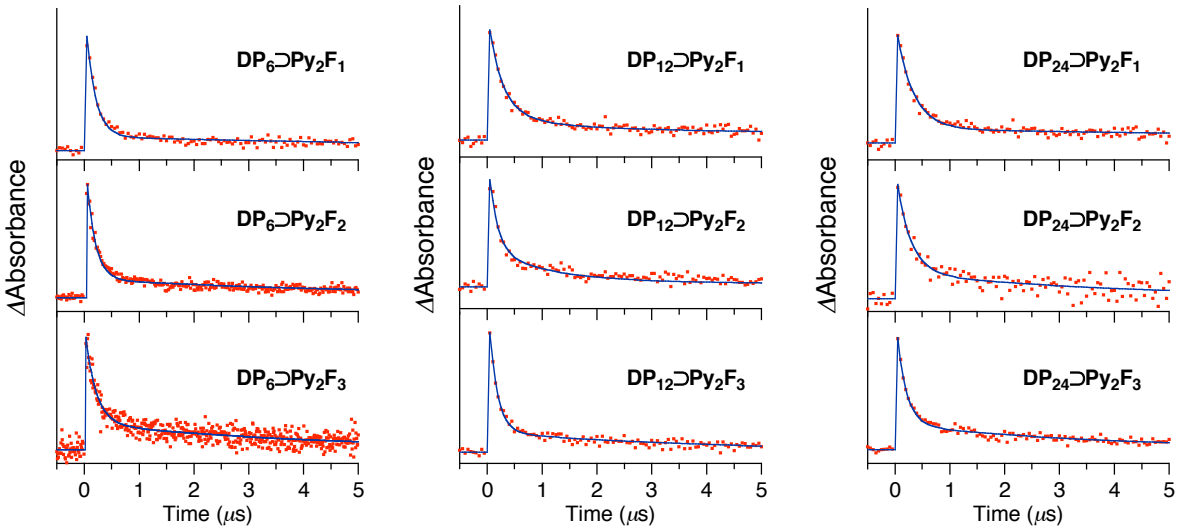

Figure S19. Transient absorption decay profiles at 1000 nm (anion radical of fullerene) of DP_6, DP_{12}, and DP_{24} in the presence of Py_2F_1, Py_2F_2, and Py_2F_3, respectively ([zinc porphyrin] = 1.0×10^{-4} M, [pyridine]/[zinc porphyrin] = 1), upon excitation at 532 nm in CH_2Cl_2 at 20 ºC.

12. Fluorescence Lifetimes (τ_f), Charge-Separation Rate Constants (k_{CS}), Charge-Separation Quantum Yields (Φ_{CS}), Charge-Recombination Rate Constants (k_{CR}), Lifetimes of Radical Ion Pair (τ_{RIP}), and k_{CS}/k_{CR} of $DP_m\supset Py_2F_n$ (m = 6, 12, and 24; n = 1–3) and $P_1\supset Py_2F_n$ (n = 1–3) and in CH_2Cl_2 at 20 °C

Complex	τ_f (ps)[a]	k_{CS} ($\times 10^9$ s^{-1})	Φ_{CS}	k_{CR} ($\times 10^6$ s^{-1})	τ_{RIP} (ns)	k_{CS}/k_{CR}
$P_1\supset Py_2$	2200 (100)					
$P_1\supset Py_2F_1$	1300 (92), 2200 (8)	0.31				
$P_1\supset Py_2F_2$	610 (72), 2200 (28)	1.2				
$P_1\supset Py_2F_3$	570 (77), 2200 (23)	1.3				
$DP_6\supset Py_2$	1600 (100)					
$DP_6\supset Py_2F_1$	320 (68), 1100 (32)	2.6	0.82	5.9	170	450
$DP_6\supset Py_2F_2$	170 (80), 720 (20)	5.0	0.89	6.4	160	770
$DP_6\supset Py_2F_3$	150 (85), 810 (15)	5.7	0.90	6.7	150	850
$DP_{12}\supset Py_2$	310 (47), 1600 (53)					
$DP_{12}\supset Py_2F_1$	130 (76), 540 (22), 1930 (2)	6.7	0.86	4.5	220	1500
$DP_{12}\supset Py_2F_2$	65 (82), 320 (13), 1800 (4)	14	0.93	6.7	150	2200
$DP_{12}\supset Py_2F_{33}$	62 (84), 420 (11), 1900 (5)	15	0.94	6.7	150	2300
$DP_{24}\supset Py_2$	300 (64), 1400 (36)					
$DP_{24}\supset Py_2F_1$	54 (94), 460 (4), 1600 (2)	17	0.92	6.3	160	2700
$DP_{24}\supset Py_2F_2$	46 (84), 260 (12), 1500 (4)	20	0.93	6.3	160	3300
$DP_{24}\supset Py_2F_3$	41 (79), 300 (16), 1600 (5)	23	0.94	6.7	150	3400

[a] Numbers in parentheses are relative amplitudes in %.